Institut für Veterinärphysiologie
der Vetsuisse-Fakultät Universität Zürich

Direktor: Prof. Dr. med. vet. Max Gassmann

Arbeitsgruppe: Prof. Dr. med. vet. Thomas Lutz

Arbeit unter wissenschaftlicher Betreuung von
Dr. Christelle Le Foll

Role of glial inflammation and cytokine production in regulating food intake and energy homeostasis in diet-resistant and diet-induced obese rats

Inaugural-Dissertation

zur Erlangung der Doktorwürde der
Vetsuisse-Fakultät Universität Zürich

vorgelegt von

Luca Papini

Tierarzt
von Lugano, Schweiz

genehmigt auf Antrag von

Prof. Dr. med. vet. Thomas Lutz, Referent
Prof. Dr. Wolfgang Langhans, Korreferent

2021

Table of content

Summary

Zusammenfassung (English)
Luca Papini
Vetsuisse-Faculty, University of Zurich 2021
E-mail: dekanat@vetadm.uzh.ch

Role of glial inflammation and cytokine production in regulating food intake and energy homeostasis in diet-resistant and diet-induced obese rats

The obesity and type 2 diabetes epidemic is escalating and represents one of the most costliest biomedical challenges facing modern society. To counter this growth, the research is centered on the continuous exploration of new therapeutic approaches.

The focus of this study is on the mechanisms underlying the role of astrocytes and microglia in the control of eating and body weight. The first aim of this study is to determine the effect of an acute high energy diet (HE) on glial activation and cytokine production in diet induced obese (DIO) and diet resistant (DR) rats and to assess whether sex-differences influence glial inflammation. Second, we aim to investigate the effect of inhibiting the IKKβ signaling pathway in the mediobasal hypothalamus astrocytes of DIO and DR rats on metabolism.
Our results revealed no differences in GFAP and Iba1 density between male and female DIO and DR rats on chow and after 3d of HE diet. Further, our in vitro experiment provided evidence that ventromedial hypothalamus (VMH) astrocyte cytokine production is increased already 24 hours after the exposure to long chain fatty acids (LCFA) and that unsaturated fatty acids (FA) can elicit a more potent anti-inflammatory response compared to saturated ones, which have instead demonstrated a pro-inflammatory effect. Finally, our data demonstrated the NF-Kβ/IKKβ pathway as a pivotal signal in altering food intake and body weight gain in DIO rats.

Keywords

1. Glial cells
2. Body weight
3. Food intake
4. Obese Rats

Zusammenfassung

Luca Papini
Vetsuisse-Fakultät Universität Zürich 2021
Institute für Veterinärphysiologie
E-mail: dekanat@vetadm.uzh.ch

Rolle der Entzündung in Glia-Zellen und von Zytokinen bei der Regulation der Nahrungsaufnahme und der Energiehomöostase bei diät-resistenten und diät-induzierten adipösen Ratten

Der Fokus dieser Studie liegt auf den Mechanismen, die der Rolle von Astrozyten und Mikroglia bei der Kontrolle der Nahrungsaufnahme und des Körpergewichts zugrunde liegen. Das erste Ziel dieser Studie war es, den Effekt einer akuten energiereichen Diät (HE) auf die gliale Aktivierung und Zytokinproduktion bei diät-induzierten adipösen (DIO) und diät-resistenten (DR) Ratten zu bestimmen und zu beurteilen, ob der Geschlechtsunterschied die gliale Entzündung beeinflusst. Zweitens wollten wir den Effekt der Hemmung des IKKβ-Signalwegs in Aostrozyten des mediobasalen Hypothalamus von DIO- und DR-Ratten auf den Stoffwechsel untersuchen.

Unsere Ergebnisse zeigten keine Unterschiede in der GFAP- und Iba1-Dichte zwischen männlichen und weiblichen DIO- und DR-Ratten unter Chow (Standard-Rattenfutter) und nach 3 Tagen mit HE-Diät. Darüber hinaus lieferte unser in vitro-Experiment den Beweis, dass die Zytokinproduktion der Astrozyten aus dem ventromedialen Hypothalamus (VMH) bereits 24 Stunden nach der Exposition gegenüber langkettigen Fettsäuren (LCFA) erhöht ist und dass ungesättigte Fettsäuren (FA) eine stärkere entzündungshemmende Reaktion hervorrufen können als gesättigte, die stattdessen eine pro-inflammatorische Wirkung gezeigt haben. Letztendlich zeigten unsere Daten, dass der NF-Kβ/IKKβ-Signalweg ein zentrales Signal bei der Veränderung der Nahrungsaufnahme und der Körpergewichtszunahme bei DIO-Ratten ist.

Schlüsselwörter

1. Gliazellen
2. Körpergewicht
3. Nahrungsaufnahme
4. Adipöse Ratten

1. Introduction

1.1 Obesity and body weight homeostasis

According to the latest available data published by the World Health Organization regarding the global prevalence of obesity in people aged 18 years and over, in 2016 39% of men and 39% of women were overweight. In the same year, 18% of children and adolescents between 5 and 19 years of age were overweight or obese. Nowadays obesity is defined as a public health problem. This pathophysiological state not only impacts on the social and psychological life of those affected, but also represents a major risk factor for the development of comorbidity conditions, including cardiovascular diseases, hypertension and stroke, diabetes mellitus as well as certain forms of cancer.

Obesity is the result of an imbalance between the amount of food eaten and the amount of energy used (Schwartz et al. 2017). On the contrary, when our body achieves to balance these parameters, we speak of energy homeostasis and consequently of body weight homeostasis. One of the key regions that is responsible for the maintenance of body weight and energy homeostasis is the hypothalamus (Ávalos et al. 2018; Seong et al. 2019). Within the hypothalamus and more specifically the arcuate nucleus (ARC), nutrients and hormones sensing-neurons (Levin et al. 2011, Ferrario et al. 2016) are able to detect variation of circulating fatty acids, glucose, peptides (e.g. glucagon-like peptide-1 [GLP-1], ghrelin) and hormones (e.g. insulin, leptin), as well other metabolically related signaling molecules such as ketone bodies (KB) (Levin et al. 2011, Ferrario et al. 2016). Using these signals, ARC neurons can monitor nutrient availability and alter their own activity to adjust the metabolic rate and mechanisms such as hunger and satiety to maintain energy homeostasis. In addition, not only neurons but also glial cells are reported to have an important role in controlling body weight homeostasis (Douglass et al. 2017, Kim et al. 2019).

1.2 Glial cells

More than half of the central nervous system (CNS) is constituted by glial cells (Kim et al. 2019). Within the CNS, four different known types of glia exist: oligodendrocytes, ependymal cells, astrocytes and microglia. Our current study will focus mainly on the latter two. Both astrocytes and microglia are continuously communicating with each other and create tight

connections with neurons to fulfill various physiological functions during brain development and throughout life (Vainchtein and Molofsky 2020). Astrocytes serves as storage for glycogen in the brain (Eduardo E Benarroch 2010, Lee et al. 2020), which can be used as endogenous energy source for neurons after his metabolism into lactate. Previous studies have also shown that astrocytes release different molecules, such as thrombospondin 1 and 2, glypicans 4 and 6, and SPARC-like protein 1 that promote the formation of synapses (Tran and Neary 2006, Vainchtein and Molofsky 2020). Furthermore, astrocytes are responsible for the formation and preservation of the blood-brain barrier (Souza et al. 2019). Their anatomical localization close to the blood vessels facilitates the regulation of neurovascular coupling (Douglass et al., 2016). Indeed, astrocytes can create a tight relationship with neurons and endothelial cells to better modulate nutrient uptake and metabolism. Microglia responds as first-responders to CNS damage caused by ischemia, pathogens or damage to neurons (Douglass et al. 2017). Once activated, they produce pro-inflammatory cytokines and perform phagocytic functions in the CNS.

1.3 Fatty acids and ketone bodies neuronal sensing

There is evidence that fatty acids (FAs) are acting as signaling molecules for hypothalamic neurons (Young J.K. 2002, Obici et al. 2002, Obici et al. 2003, Dragano et al. 2018). Indeed, long chain FAs (LCFAs) can bind to the fatty acid receptor CD36 and be used as signaling molecules by metabolic sensing neurons of the ARC and the ventromedial nucleus (VMN) (Le Foll 2016). It has been further demonstrated that during short-term high-fat diet (HFD) feeding conditions in rats, free fatty acids (FFA) are uptaken from the circulation by astrocytes and used to produce KB. Once produced by astrocytes, KB can override CD36-mediated FA sensing and quickly decrease food intake (FI). However, if HFD is consumed over a longer period of time, this mechanism becomes attenuated. Our overarching hypothesis is that the HFD-induced gliosis alters the capacity of neurons to respond to FA and KB due to the secretion of cytokines. Here we will try to establish a timeline of these events and first, we will assess the effect of short-term HFD on astrocyte metabolism and morphology.

1.4 Gliosis and hypothalamic inflammation induced by high-fat feeding

As a reaction to HFD, both astrocytes and microglia may exhibit a hypertrophic and reactive phenotype known as gliosis (Dorfman 2015). In such a case, the expression of the glial fibrillary acidic protein (GFAP) and ionized calcium-binding adapter molecule 1 (Iba1) will be consequently upregulated (Sinha 2017). GFAP is mainly expressed by the astrocytes and the ependymal cells, while Iba1 is specifically expressed in microglia (Dong and Benveniste 2001, Sasaki 2001). Once activated, astrocytes and microglia can secrete pro-inflammatory cytokines such as IL-6, IL-β and TNF-α (Tha et al. 2000, Wang et al. 2015, Seong 2019). Similar to rodents, Thaler et al. (2012) found evidence of gliosis using MRIs examination in the hypothalamus of people affected by obesity.

It has been recently shown that HFD increases the expression of hypothalamic cytokines before weight gain appears (Ávalos et al. 2018, Cansell et al. 2020). According to the study of Cansell et al., hypothalamic inflammation could occur already in the first hours after HFD feeding. This then leads to the activation of hypothalamic glial cells (Ávalos et al. 2018), which will themselves contribute to the progression of the inflammatory cascade. The major signaling pathway in the regulation of gliosis and the subsequent production of inflammatory peptides involves the NF-kβ/IKKβ complex (Ávalos et al. 2018, Seong 2019). Indeed, consumption of long-chain saturated fatty acids (SFAs) induces endoplasmic reticulum (ER) stress via toll-like receptor (TLR4) and subsequent c-Jun N-terminal Kinase (JNK) activation. ER stress trigger IKKβ, causing activation of NF-kB, an essential transcription factor for inflammatory responses (Giuliani 2001). Nowadays there is evidence that TLR4 is expressed by both astrocytes and microglia (Gorina et al. 2011, Zhao 2016). In addition, a previous study by Douglas et al. (2017) showed that temporal depletion of IKKβ in mice after 6 weeks of HFD feeding prevented the further development of HFD-induced astrogliosis and glucose intolerance.

1.5 DIO and DR rat model

The following experiments will use the model of selectively bred diet-induced obese (DIO) and diet-resistant (DR) rats as a model of human obesity and diabetes. This model of obesity has been well characterized over the years (Levin et al. 1986, Levin et al. 2003b, Le Foll et al. 2015b) and is successfully established in our lab. These rats are selectively bred to produce polygenically-inherited diet-induced obesity or to remain lean ("diet-resistant") when fed HFD

(Ricci et al. 2003). As in most human obesity (Stunkard 1991, Bouchard 1997), the DIO phenotype is inherited as a polygenic trait (Levin et al. 2003a). The advantages of using DR and DIO rat model is that, contrary to outbred rats, the selective breeding allows us to separate DR and DIO rats even before they go under chronic HFD regiment in order to identify key metabolic alterations that lead to the development of obesity; further, DR rats serve as a dietary control since they eat the same HFD but do not become obese or develop the metabolic and hormonal sequelae of obesity as do DIO rats.

2. Hypothesis and Aims

2.1 Hypothesis

After 3d of HFD or high energy diet (HE) diet feeding, even though DIO rats present elevated VMH KB they are not able to reduce their caloric intake to the level of chow diet intake as DR rats (Le Foll et al. 2015b). We thus hypothesize that:
Inflammatory cytokines prevent KB to alter neurons' activity and will therefore blunt ketone effects on neuronal FA sensing and contribute to onset of the DIO obese phenotype.

2.2 Aim

1) Our first aim will determine the effect of an acute HE diet on glial activation and assess whether sex-differences affect hypothalamic glial inflammation in DIO and DR rats.

2) Our second aim will assess the relative production of cytokines in cultured DIO and DR ventromedial hypothalamus' (VMH= ARC+VMN) astrocytes after 1 to 4 days of LCFA vs. no LCFA exposure. The most abundant FA present in the HE diet will be tested here.

3) Our last aim will examine the inhibition of astrocytes' inflammatory pathway in DIO and DR rats. We postulate that this will restore the KB neuronal sensing in DIO rats fed HFD and prevent the development of obesity.

3. Material and Methods

3.1 DIO and DR rats breeding and housing conditions

The breeding of both DIO and DR rats started about 2 years ago in the animal facility of our institute. The generation F5-F6-F7 were used in the following experiments. Rats were kept in T2000 macrolon cages in an environmentally controlled room where temperature was set at 21°C (± 2 °C) with a light cycle of 12h (Lights off at 10:00h). Rats were kept in an enriched environment with wood chip bedding, tissue for nesting, plastic tubes and plastic houses. Food and water were provided ad libitum. Unless otherwise specified, the animals were fed a standard chow diet (Diet 3436, Provimi Kliba AG, Kaiseraugst, Switzerland; energy content: 3.15 kcal/g, 65.4% energy from carbohydrates, 12.3% from fat and 22.4% from protein as percent of total energy content). Handling, measurement of body weight and food intake were conducted weekly. 10 DR and 10 DIO were bred at each generation. At postnatal day 2 (P2), litters were normalized to 5 males and 5 females. At weaning, 1 male and 1 female from each litter were taken for each experiment.
All procedures were approved by the Veterinary Office of the Canton Zurich, Switzerland.

3.2 Experiment 1

3.2.1 Animals

At a weaning age of 21 days, 64 DIO and 64 DR male and female rats were group housed (n=3-4/cage) in T2000 macrolon cages. At 11-week-old, 26 DIO and 26 DR rats (n=13 male and 13 females/phenotype) were switched to a HE diet for 3 days (Diet D12266B, Research Diets, Inc., New Brunswick, USA; energy content: 4.4 kcal/g, protein: 18.5%, carbohydrates: 56.7%, fat: 15.6%) while 26 DIO and 26 DR (n=13 male and 13 females/phenotype) rats were maintained on chow diet. A third group of rats fed HE diet (n=6 male and 6 females/phenotype) was pair-fed with the chow diet group. In other words, the HE diet pair-fed rats received the same amount of calories as the chow diet group had eaten the previous day. Daily body weight and food intake were measured.

3.2.2 Terminal perfusion

After a 2h fast before dark onset, the animals were injected with pentobarbital (100 mg/kg) diluted 1:1 with 0.9% saline solution to achieve a deep anesthesia before perfusion. Trans-cardiac perfusion was performed with 0.1 M phosphate buffer (PB) for 1.5 minutes followed by 4% paraformaldehyde (PFA) for 2.5 minutes. PB and PFA were pre-cooled to 4°C and kept on ice during the perfusion. Brains were removed and kept in 4% PFA overnight, followed by an overnight incubation in 20% sucrose-PB solution. Brains were separated between cerebrum and cerebellum and both parts were frozen in hexane on dry ice (approximately -80°C) for 2.5 minutes. Thereafter, the brains were stored at -80°C until further processing.

3.2.3 Brain sectioning

Brains were serially sectioned into 4 series of 25 µm thick slices throughout the ARC from brain levels -1.32 to -3.60 mm using the bregma reference (Paxinos & Watson, 2007) with a cryostat (CM3050S, Leica Biosystems, Germany) set at an object temperature of -19°C and a chamber temperature of -21°C. Brain sections were collected and mounted on Superfrost Plus slides (Thermo Fisher Scientific, Reinach, Switzerland). Slides were kept in cryoprotectant at -20°C (50% 0.02M potassium phosphate buffered saline (KPBS), 30% ethylene glycol, 20% glycerol) until further processing.

3.2.4 GFAP and IBA1 immunofluorescence staining

GFAP

Brain sections were rinsed in 0.01 M phosphate-buffered saline (PBS) five times for 5 minutes. To reduce background signal, brain sections were then blocked for 2 hours in a solution of 0.3% Triton X, 1% bovine serum albumin (BSA) and 2% normal donkey serum (NDS) in PBS at room temperature. The brain sections were then incubated for 48 hours in 0.3% Triton X, 1% BSA and 2% NDS in PBS with primary antibody goat anti-GFAP (1:500; ab53554, Abcam) at 4°C. After rinsing the sections in PBS five times for 5 minutes, they were incubated in 0.3% Triton X and 2% NDS in PBS with secondary antibody Cy3 donkey anti-goat (1:100; 705-165-147, Jackson ImmunoResearch). The slides were rinsed in PBS three times for 5 minutes, followed by 4 minutes counterstaining in DAPI (0.25 µg/ml; 62248, Thermo Fisher Scientific).

After rinses in PBS five times for 5 minutes, slides were coverslipped with approximately 80 µl mountant solution (CitiFluor, 17970-100, Electron Microscopy Sciences). Immunostained slides were then stored at 4°C until imaging.

Iba1

After rinsing slides in PBS five times for 5 minutes, brain sections were blocked in 0.3% Triton X, 1% BSA and 2% NDS in PBS at room temperature for 2 hours. The brain sections were then incubated for 48 hours in a solution with 0.3% Triton X, 1% BSA and 2% NDS in PBS with primary antibody rabbit anti-Iba1 (1:000; 019-19741, Wako) at 4°C. After rinsing the slides in PBS five times for 5 minutes, the slides were incubated for 2 hours in a solution with 0.3% Triton X and 2% NDS in PBS with secondary antibody Alexa fluor 488 goat anti-rabbit (1:100; 111 545-144, Jackson ImmunoResearch) at room temperature. The slides were rinsed in PBS three times for 5 minutes, followed by 4 minutes counterstaining in DAPI (0.25 µg/ml) and 5 final rinsing steps in PBS for 5 minutes were performed. Last, slides were coverslipped and stored as above.

3.2.5 Brain imaging and quantification

Immunostained sections were visualized with an Axio Imager 2 microscope (Carl Zeiss, Feldbach, Switzerland) using a 20x objective and two sections per rat were selected at the level of the ARC. Each ARC section was imaged at the lateral and ipsilateral side. Density per area of GFAP and Iba1 was quantified by ImageJ particle analysis (Fiji). The threshold was set at the average optimal threshold of all slides (GFAP: 150; Iba1: 150).

3.2.6 Singleplex Assay - measurement of leptin in plasma

A U-PLEX® Metabolic Group 1 (Rat, Meso Scale Diagnostics) singleplex assay was used to measure the plasma leptin level of DIO and DR rats. All reagents were brought to room temperature before beginning with the protocol. 200 µl of biotinylated capture antibody were added to 3.3 ml of Diluent 100. The solution was mixed by vortexing and 25 µl were added to each well of the provided MSD GOLD Small Spot Streptavidin Plate afterwards. After 1h of incubation, the plate was washed 3 times with 150 µl/well of 1X MSD Wash Buffer (PBS-Tween 0.05%).

For the preparation of the Metabolic Assay Working Solution, 6'965 µl of Diluent 13 and 35 µl of aprotinin were combined in a 15 ml tube. This solution was used for preparing the calibrator and the controls: the calibrator was reconstituted by adding 250 µl of Metabolic Assay Working Solution to the glass vial; standards were made by serial dilution. The prepared standards and the samples were added to the wells according to the plate diagram (50 µl of each). The plate was then incubated at room temperature with shaking for 2 hours. After this time, the plate was washed 3 times with 150 µl/well of 1X MSD Wash Buffer. After the washing, 50 µl of detection antibody solution (60 µl of SULFO-TAG™ Conjugated Detection Antibody combined with 5'940 µl of Diluent 11) were added to each well. The plate was then sealed with an adhesive plate seal and incubated at room temperature with shaking for 1 hour. After 1 hour, the plate was washed 3 times with 150 µl/well of 1X MSD Wash Buffer and 150 µl/well of MSD GOLD Read Buffer A were added afterwards. The plate was analyzed and processed on the MSD instrument.

3.3 Experiment 2

3.3.1 Hypothalamic Astrocytes isolation

The day before cell culture four 75 cm^2 flasks were coated over night with poly-D-lysine (50 µg/ml – Sigma P6407). The next day they were rinsed 3 times with cell culture water. 3-4 weeks old rats of each group (DIO vs. DR, males and females) were sacrificed using pentobarbital (100 mg/kg). The brains were kept in PBS on ice and once under the cell culture hood transferred into clean PBS dish. The mediobasal hypothalami were then isolated and transferred into a 35 mm dish was filled with 5 ml of Neurobasal media (Table 1). The tissues were cut into small pieces and were transferred into a 15 ml tube. Tissues were triturated using 3 Pasteur pipettes with large, medium and small opening. After each trituration the remaining tissue chunks were let to settle for 3 min and the suspension was transferred to a new 15 ml tube and 2.5 ml of Neurobasal media were added before the next trituration. At the end of the 3rd trituration the tube was filled with Neurobasal media to 15 ml. The cell suspension was finally transferred into the 75 cm^2 flask and the volume of Neurobasal adjusted to 20 ml. The flask was put into the incubator and the media changed every 3-4 days until confluency (approximately 10-12 days). The day before astrocyte separation, for each flask of astrocytes in culture, one 75 cm^2 flask and six 6-wells plates were coated with poly-D-lysine (50 µg/ml). The day of

astrocytes separation, the flask was shaken at 37°C, 250 rpm for 3-4h hours. The media was then aspirated and cells were rinsed 3 times with sterile PBS in order to get rid of oligodendrocytes and microglia. 5 ml of Trypsin/EDTA 0.05% (Invitrogen, 25300-054) were added afterwards. To accelerate the action of trypsin, the flask was put in the incubator for 2 min. The cell suspension was transferred into a 50 ml tube and 10 ml of Neurobasal 5 mM were added. Before the next step, the flask was rinsed one time with 5 ml of Neurobasal 5 mM. The cell suspension was centrifuged for 5 min, 1500 rpm at room temperature. The pellet was resuspended in 20 ml Neurobasal 5 mM and the cell suspension centrifuged another time for 5 min, 1500 rpm at room temperature. After the second centrifugation the pellet was resuspended into 5 ml Neurobasal 5 mM (Le Foll et al. 2015c). Finally, the astrocytes were replated in six 6-well plates and 1 flask for backup. 100 µl of astrocytes were added in each well.

3.3.2 Preparation of cell culture media

Neurobasal A-P/S

For the preparation of 500 ml of Neurobasal A-P/S: 5 ml P/S (10,000 U/ml, Sigma P-0781), 100 µl Gentamicin (Sigma G1397, 50 mg/ml) for a final concentration of 10 µg/ml, 50 ml FBS (heat inactivated) for a final concentration of 10%, 0.450 g Glucose (Sigma, G-7021) for a final concentration of 5 mM, 0.126 g Pyruvic Acid (Sigma, P-3662) for a final concentration of 0.23 mM, 4 g Sucrose (Sigma S-5016) to adjust Osmolarity to 260 ± 5 and Neurobasal-A to 500 ml (Invitrogen, no glucose, no pyruvate, A24775-01) were added. The entire solution was filtered under the hood using a 500 ml 0.2 µm filter set. The final media was stored at 4°C until further use.

Neurobasal-No serum-2.5 mM glucose

For the preparation of 100 ml of Neurobasal-No serum-2.5 mM glucose: 0.5 ml P/S (10,000 U/ml, Sigma P-0781), 20 µl Gentamicin (Sigma G1397, 50 mg/ml) for a final concentration of 10 µg/ml, 0.045 g Glucose (Sigma, G-7021) for a final concentration of 5 mM, 0.0252 g Pyruvic Acid (Sigma, P-3662) for a final concentration of 0.23 mM, 0.8 g Sucrose (Sigma S-5016) to adjust Osmolarity to 260 ± 5 and Neurobasal-A to 100 ml (Invitrogen, no glucose, no pyruvate, A24775-01) were added. The entire solution was filtered under the hood using a filter set. The final media was stored at 4°C until further use.

3.3.3 Fatty acids dilution

For the preparation of [10mM] stock of Oleic acid (18:1(9) n-9 MW=282.5 g/mol Sigma Ref O1257): 3.540 ml of sterile H2O were added to the bottle. The resulting solution was then diluted 1:10 by adding 200 µl of [10mM] stock to 1'800 µl PBS. [13 µM] were added on astrocytes.

For the preparation of [10mM] stock Linoleic acid (18:2(9,12) n-6 MW=280.5 g/mol Sigma Ref L5900): 3.560 ml of sterile H2O were added to the bottle. The resulting solution was then diluted 1:10 by adding 200 µl of [10mM] stock to 1'800 µl PBS. [13 µM] were added on astrocytes.

For the preparation of [10mM] stock of Palmitic acid (C16:0 MW=256.5 g/mol Sigma P5585): 2.56 mg were diluted in 100 µl DMSO and then added to the solution obtained from 900 µl PBS plus 0.1 g BSA Free FFA. [73 µM] were added on astrocytes.

For the preparation of [10mM] stock of Stearic acid C18:0 MW=284.2 g/mol Sigma Ref S4751: 3.06 mg were diluted in 100 µl DMSO and then added to the solution obtained from 900 µl PBS plus 0.1 g BSA Free FFA. [73 µM] were added on astrocytes.

The Vehicle BSA contains the DMSO and BSA similar to PA and SA solutions.

NB: all the astrocytes were first treated in a pilot study with [73 µM] but this concentration of OA and LA was too high and killed them.

3.3.4 Fatty acids treatment and sample harvesting

The day before the experiment (about 2-3 days after replating in wells), when astrocytes were 70-80% confluent, the cells were washed with PBS and Neurobasal- 2.5 mM glucose media without serum was added afterwards. For each of the 4 groups (DIO vs. DR, males and females), six 6 well-plates were used and the following treatments were performed: vehicle alone, vehicle with BSA, oleic acid, linoleic acid, palmitic acid, stearic acid (n=6/treatment). The day of the experiment, before adding any fatty acid, 100 µl of medium were harvested for Time 0. After doing this, 13 µM oleic acid and 13 µM linoleic acid (or the same volume of media in the vehicle treated group), respectively 73 µM palmitic acid and 73 µM stearic acid (or the same volume of BSA in the vehicle with BSA treated group) were added in the corresponding plate. For each time point, 100 µl of medium were harvested and frozen at -80°C. After each harvest process, 13 µM oleic acid and 13 µM linoleic acid (or the same volume

of media in the vehicle treated group), respectively 73 μM palmitic acid and 73 μM stearic acid (or the same volume of BSA in the vehicle with BSA treated group) and 100 μl of fresh media to compensate were added in the corresponding plate. The last day of the experiment, after the last time point, the cells were washed with 2 ml of cold PBS. 250 μl LBA+TG buffer (Promega) was added to each well to lyse the cells. The lysates were collected and frozen at -80°C until mRNA extraction.

In order to test whether saturated fatty acids increased the concentration of cytokines compared to unsaturated even at equal concentration, we performed a supplementary experiment where astrocytes of DR males were treated with either 10 μM oleic acid (or the same volume of media in the vehicle treated group) and 10 μM palmitic acid (or the same volume of BSA in the vehicle with BSA treated group).

3.3.5 MSD Cytokine Assay

For the measurement of the inflammatory biomarkers a V-Plex assay (MSD® Multi-Spot Assay System, proinflammatory Panel 2 (rat) kit) was used.
All plates and diluents were brought to room temperature. 150 μL of blocker H solution were added in each well. The plate was sealed and incubated at room temperature 1h on shaker (300-1000 rpm). In the meantime, the calibrators were prepared: the lyophilized control 1 was reconstituted in 1000 μl of Diluent 42. The next calibrator was prepared by transferring 100 μl of the highest calibrator to 300 μl of Diluent 42. The 4-fold serial dilutions were repeated 5 additional times to generate 7 calibrators. Diluent 42 was used as the zero calibrator. After 1h on shaker, the plate was washed 3 times with 150 μl/well wash buffer (PBS-Tween 0.05%). 50 μl/well standards or samples were added afterwards and incubated at room temperature on shaker for 2h (300-1000 rpm). In the meantime, the detection antibody solution was prepared by adding 60 μl of each antibody (SULFO-TAG Anti-rat IFN-γ; SULFO-TAG Anti-rat IL-10; SULFO-TAG Anti-rat IL-β; SULFO-TAG Anti-rat IL-6; SULFO-TAG Anti-rat TNF-α) to 2700 μl of Diluent 40. After 2h on shaker, the plate was washed 3 times with 150 μl/well wash buffer. After, 25 μl/well Detection antibody solution were added. The plate was then incubated at room temperature for 2h on shaker (300-600 rpm). The plate was washed 3 times with 150 μl/well wash buffer. Finally, 150 μl of 2X MSD read buffer T (10 ml of read T buffer plus 10 ml of ddH_2O) was added to each well and the plate was read on MSD equipment.

3.4 Experiment 3

3.4.1 Animals

18 DIO and 18 DR males were recruited for this experiment. At an age of 3-week-old, 9 DIO and 9 DR were injected in the medio basal hypothalamus with an AAV GFAP-IKKβ shRNA virus (ssAAV-9/2-hGFAP-hHBbI/E-chI[4xsh(rIKKb)]-EGFP-WPRE-bGHp(A) custom made by the Viral vector core UZH), while the remaining animals with a control (ssAAV-9/2-hGFAP-hHBbI/E-chI[4x(shm/rNS)]-EGFP-WPRE-bGHp(A) scrambled) virus. The AAV GFAP-IKKβ shRNA virus is composed of 4 shRNA sequences and has the characteristic of specifically inhibiting the expression of IKKβ in astrocytes due to its GFAP promoter. After surgery, animals were single housed with nesting and housing materials. Animals were kept on chow diet for 1 week during recovery and then switched to 45% fat diet (HFD) for 7 weeks (Diet D12451, Research Diets, Inc., New Brunswick, USA; energy content: 4.7 kcal/g, protein: 20%, carbohydrates: 35%, fat: 45%).

3.4.2 Stereotaxic virus injection in the mediobasal hypothalamus

Meloxicam (Metacam ® 2 mg/kg, s.c.) and 2,5% Baytril ® injectables (10 mg/kg, s.c.) were given to the animal 20-30 minutes before the surgery. The anesthesia was performed using a combination of ketamin (Ketanarkon ® 40 mg/kg, s.c.) and medetomidine (Medetor ® 0,8 mg/kg, s.c.). After induction, vitamin A ointment was applied to the eyes. The head and neck of the animal were shaved. The head of the animal was secured in ear bars of stereotaxic frame afterwards. The skin was then sterilized with Betadine ® and a small incision along the sagittal line of the skull was made. Periosteum and connective tissue were removed from the skulls surface. The height of bregma in relation to lambda was verified and leveled and if necessary, the head readjusted to increase the accuracy of stereotaxic procedures. Established stereotaxic procedures to introduce the selected AAV into the brain region of interest were used. The final stereotaxic coordinates were taken from bregma: 2.6 mm posterior, ±0.3 mm lateral, and 8.5 mm ventral (the latter relative to the dura mater). The virus (2.0 x 10E12 vg/ml in 0.5 ul per side) was infused at a constant slow rate of 200 nl/min with a 33G needle. The needle was left in place for 5 additional minutes after the end of each infusion to avoid any reflux. The skull incision was sutured using Vicryl 6-0 ®. After the animal was removed from the stereotaxic apparatus, atipamezole (Revertor ® 0,7 mg/kg) was injected in order to antagonize

medetomidine. The animal was kept warm and supervised until fully awake. Metacam ® (2 mg/kg, s.c.) and 2,5% Baytril ® injectables (10 mg/kg, s.c.) were provided for 5 days.

NB: in this experiment, we injected all animals bilaterally in the ventromedial hypothalamus with the intention to achieve a knockdown in the left and right mediobasal hypothalamus. Unfortunately, post-mortem histological analysis showed the presence of the virus only on one side. This limitation is relevant for the interpretation of our findings.

3.4.3 Assessment of food intake and meal patterns

Animals were individually housed in cages equipped with BioDAQ Food Intake Monitors (Research Diet, New Brunswick, NJ, USA) to continuously measure food intake and meal patterns. Following 7 days of acclimation in the BioDAQ cages, rats were fasted for 12 h during the light phase. At dark onset (10:00 h), food was returned and baseline refeeding was measured for the subsequent 12h. Meal pattern criteria were an intermeal interval (IMI) of 900 s and a minimal meal size of 0.23 g (Duffy et al. 2018).

3.4.4 Indirect calorimetry

A 16-cage TSE PhenoMaster open circuit indirect calorimetry system was used for the determination of O_2 consumption and CO_2 production (TSE Systems; Bad Homburg, Germany). The system was calibrated using precision calibration gases prior to each run. Room air was passed through each cage at a flow rate of 0.41 L/min. Every 20 min, cage air was sampled from each individual cage and analyzed for O_2 and CO_2. From these values, energy expenditure (EE) and respiratory exchange ratio (RER) were calculated based on equations from Weir (Weir 1949). To account for differences in body weight and body mass composition, EE data were corrected for individual lean body mass (LBM in g) and fat mass (FM in g) using the following equation: $LBM + 0.2FM$, as recommended by Even and Nadkarni (Even and Nadkarni 2012, Piattini et al. 2019).

3.4.5 Oral glucose tolerance test

Food was removed 2 h prior to lights off and rats were gavaged at lights off, using an (16 Gauge) intra-gastric needle with 2 g/kg of D-glucose. Blood was sampled from the tail prior to gavage (0) and at 15, 30, 60, 90, and 120 min post-gavage for glucose measurement.

3.4.6 QPCR of the medio-basal hypothalamus and gene expression measurement

Tissue collection

Brains were mounted on the cryostat and trimmed until the beginning of the ARC starting at the brain level -1.72 mm using the bregma reference (Paxinos & Watson, 2007). Each side of the mediobasal hypothalamus (MBH) was then dissected and collected. Samples were stored at -80°C until further analysis.

RNA extraction

MBH mRNA was extracted using a Promega RNA extraction set (ReliaPrep RNA Tissue Miniprep System, Z6111; Promega, Madison, WI, USA). Briefly, 250 µl of lysis buffer (30 ml lysis buffer, 600µl thioglycerol) were added to the tissue sample. The tissue was roughly lysed by pipetting up and down with a 1000 µl pipette, followed by further lysis in a 1 ml syringe with a 25G x 16 mm needle. 85 µl 100% isopropanol was then added and the mRNA was extracted according to the manufacturer's protocol.

RNA concentration and mRNA quality (260/280 ratio) were measured by NanoDrop spectrophotometry. Samples were diluted with nuclease free water to achieve a final concentration of 0.125 µg/µl.

Reverse transcription PCR (RT-PCR)

To synthesize cDNA from mRNA, a SensiFast cDNA Synthesis Kit (SensiFAST, BIO-65054; Bioline, Memphis, TN, USA) and corresponding protocol were used. For 1 sample, 7 µl nuclease free water, 4 µl 5x reaction buffer and 1 µl reverse transcriptase were prepared as a mastermix. 12 µl were then added to 8 µl of the diluted mRNA each. Then, a RT-PCR was performed: 25°C for 10 min, 42°C for 15 min, 85°C for 5 min and 4°C to cool down.

qPCR

cDNA was diluted with 30 µl nuclease free water to achieve a final concentration of 10 ng/µl. As for the reverse transcription, a qPCR mastermix was prepared. For 1 sample, 7 µl nuclease free water, 10 µl 2x TaqMan Gene Expression Master Mix (TaqMan Fast Advanced Master Mix, 4444557, Thermo Fisher Scientific, Waltham, MA, USA), 1 µl TaqMan Gene Expression Assay of the gene of interest and 2 µl diluted cDNA were mixed. Samples were run in duplicate for all genes: GAPDH (Rn01775763_g1) and IKKb (Rn00584379_m1). The following conditions were used for the qPCR: 2 minutes 50°C hold for incubation, 2 minutes 95°C hold for polymerase activation, 40 cycles of 3 seconds 95°C denature and 30 seconds 60°C anneal/extend (7500 Fast Real-Time PCR System).

3.5 Statistics

Results were analyzed with Prism 9 using two- or three-way analysis of variance (ANOVA) followed by multiple comparison intergroup analysis. All data are expressed as mean ± SEM and any statistically significant differences are indicated by asterisks or letters.

4. Results

4.1 Experiment 1: Effect of an acute HE diet and genotype on body weight, food intake and glial activation in DIO and DR rats

4.1.1 Body weight gain and food intake in DIO vs. DR animals on chow, pair fed (HE to chow) and HE diet

In this experiment, we first measured body weight change (**Fig. 1A, B**) and body weight gain (**Fig. 1C, D**) of DR males (**Fig. 1A**) and females (**Fig. 1B**) rats compared to DIO males (**Fig. 1C**) and females (**Fig. 1D**) rats during 8 weeks of chow diet feeding from 3- to 11-week-old. At 9-week-old, baseline food intake was measured on 4 consecutive days for both males (**Fig. 1E**) and females (**Fig.1F**) rats. As expected, DIO rats gained 23% more weight and ate 18,5% more on chow diet than DR male rats. The same observation was also made in female rats. Even though DIO rats are larger than DR rats when fed a low-fat chow diet from weaning (Levin et al. 1986, Levin et al. 2002, Ricci et al. 2003), they are not fatter as seen with the comparable leptin levels on chow diet (**Fig. 2G, H**).

On HFD or HE diet the DIO strain has a predisposition to rapidly become hyperphagic, obese, leptin and insulin-resistant (Levin et al. 1986, Levin et al. 2002, Ricci et al. 2003). Most importantly, when chow-fed DIO and DR rats are fed HE diet, both overeat for 3 days. Whereas DR rats then reduce their intake to chow-fed levels on day 3 (Levin et al. 2003b, Le Foll et al. 2015b), DIO rats continue to overeat. A pair-feeding group was included to test whether the amount of kcal or just an increase in fatty acids compared to chow diet alters glial inflammation. Our results showed that over the 3d period, DIO and DR HE-fed male and female rats ate more ($P<0.001$) and tended to gain more weight compared to the chow groups (**Fig. 2A, B**). On day 2 and 3 of HE diet, DR rats reduced their caloric intake. On day 3, male DR rats ate 20 % ($P=0.0018$) and female ate 48% ($P<0.0001$) less compared to DIO rats (**Fig. 2E, F**). Even though pair-fed rats ate the same amount of kcal than chow diet rats, they lost weight compared to HE and chow diet-fed rats (**Fig. 2A, B**).

4.1.2 Measurement of leptin in chow-, 3d HE-, pair- and 4 weeks HE-diet fed DIO and DR rats

Blood samples were collected at termination and the plasma leptin concentration was measured. In addition to our samples, obtained after the sacrifice of the generation F5, DIO and DR samples taken from a previous generation (bred in our facility) that were fed HE diet for 4

weeks were analyzed. 3d HE diet fed rats (with the exception of DR females) presented an increase of leptin levels compared to chow or pair-fed groups (**Fig. 2G, H**). On chow, 3d HE diet, and 3d pair-fed groups, the concentration of leptin did not differ significantly between DIO and DR. After 4 weeks of HE diet DIO rats leptin levels were increased by almost 2-fold while DR rats showed similar values to chow, 3d HE or 3d pair-fed DR rats. Finally, we observed a higher plasma leptin concentration in male rats compared to female rats at each time point.

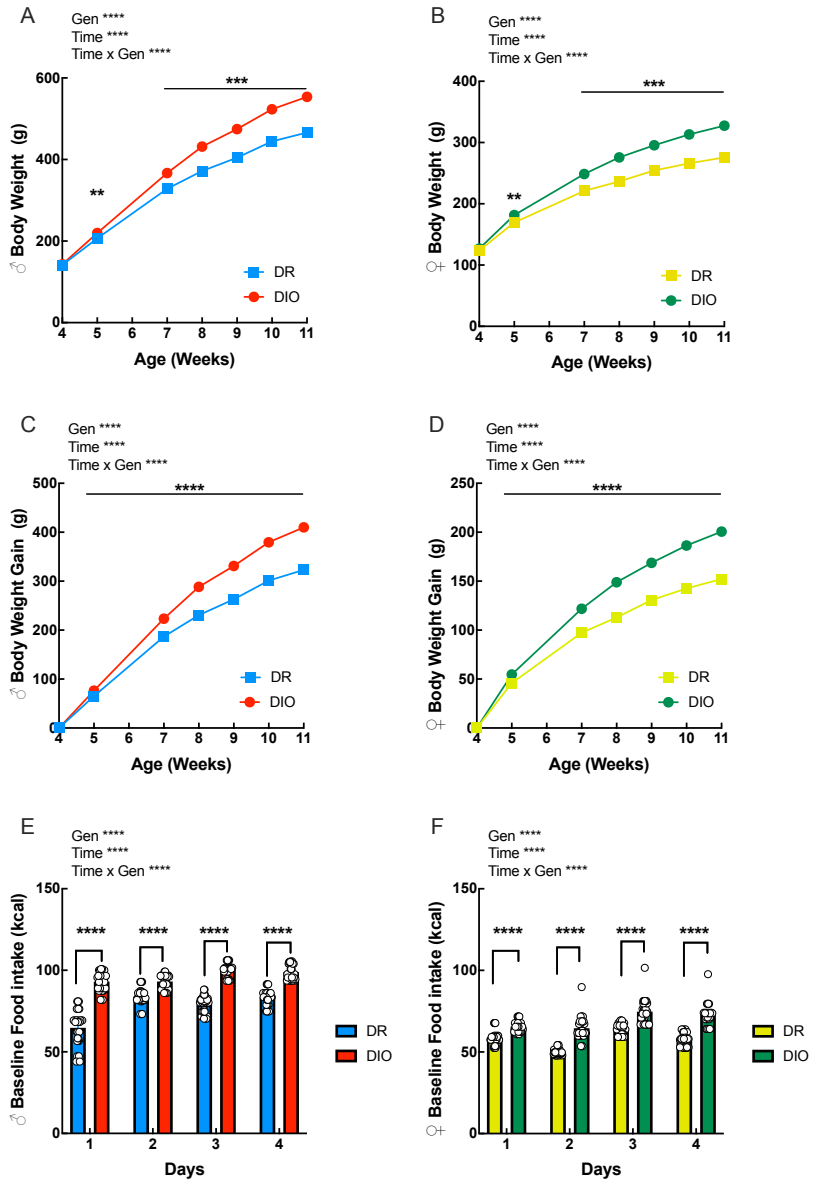

Figure 1: Body weight (A, B), body weight gain (C, D) and food intake (E, F) of diet induced obese (DIO) and diet-resistant (DR) male (A, C, E) and female (B, D, F) rats on chow. Data are represented as mean ± SEM; n = 32/group; Factors: genotype (Gen) and time. Statistics: ns > 0.05; *P ≤ 0.05; **P≤0.01; ***P≤0.001; ****P≤0.0001 by 2-way ANOVA.

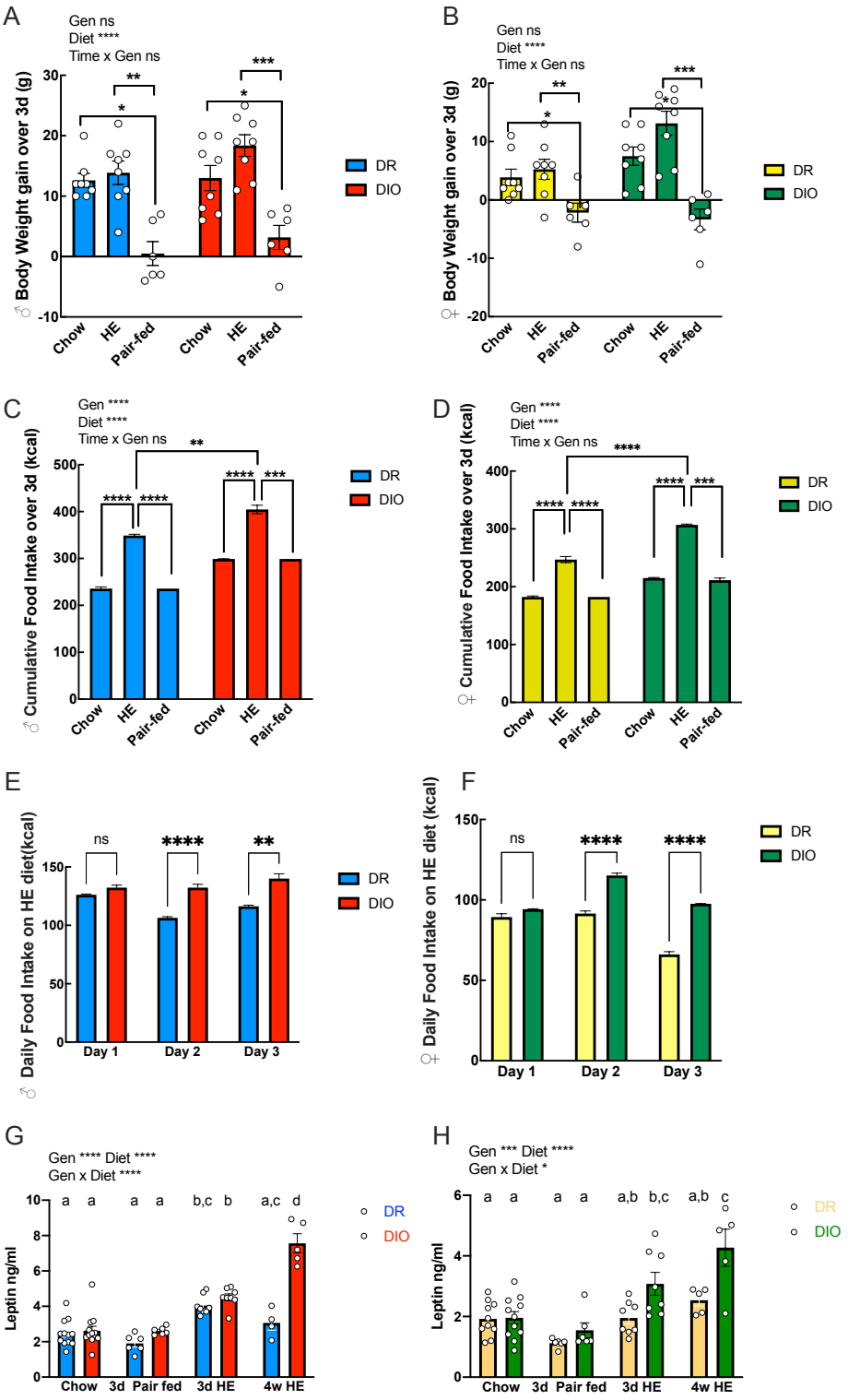

Figure 2: Body weight gain (A, B) and food intake (C, D) of DIO and DR male (A, C) and female (B, D) rats after 3 days on chow, high energy (HE) or HE-diet pair-fed. Daily food intake on HE diet of DIO and DR male (E) and female (F) rats. Leptin concentration in plasma of DIO and DR male (G) and female (H) rats after 3 days of chow, HE, HE-diet pair-fed or 4 weeks HE diet. Data are represented as mean ± SEM; n = 4-13/group. Factors: genotype (Gen), diet and time. Statistics: ns > 0.05; *P ≤ 0.05; **P≤0.01; ***P≤0.001; ****P≤0.0001 by 2-way ANOVA; data in C and D followed by Sidak multiple comparison test. G, H: (a, b, c) Data points with different superscript differ from each other by P<0.05 after multiple comparison intergroup analysis.

4.1.3 Measurement of GFAP and Iba1 density in the arcuate nucleus of the hypothalamus (ARC) in DIO and DR rats after 3 days of chow, pair-fed or HE diet

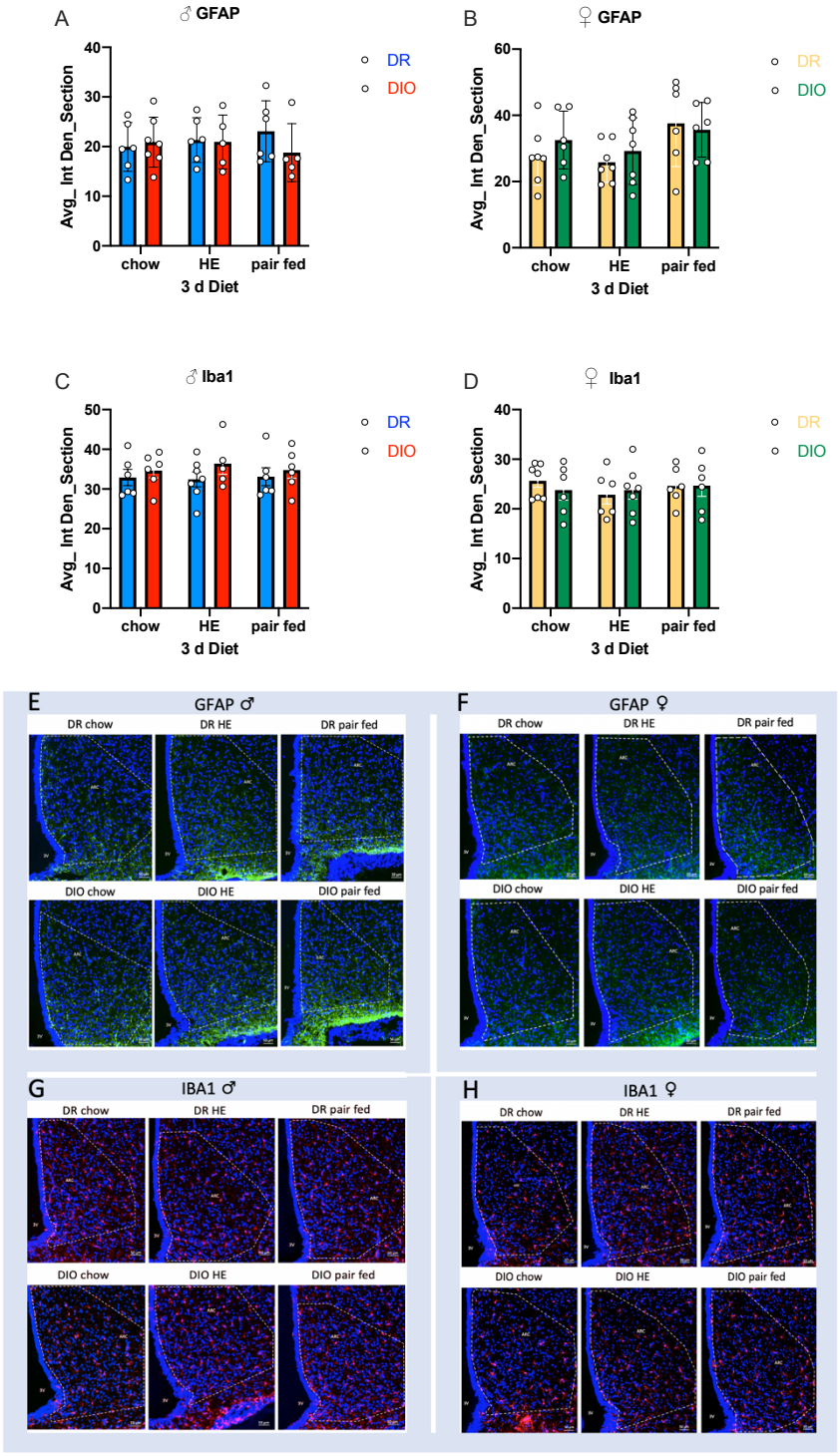

Figure 3: Density per area of GFAP (A, B) and Iba1 (C, D) in male and female DIO-DR rats fed chow or HE diet. Representative 20X image of the hypothalamic arcuate nucleus of GFAP in male rats (E), GFAP in female rats (F), Iba1 in male rats (G) and Iba1 in female rats (H). Data are represented as mean ± SEM; n = 5-7/group. Data were analyzed with two-way ANOVA.

An immunohistofluorescence staining was performed to quantify the density of GFAP and Iba1 on chow and after 3d of HE diet. The impact of genotype, sex and diet on gliosis was measured in the ARC. None of these factors had a significant difference on GFAP and Iba-1 density among all groups (**Fig. 3**).

4.2 Experiment 2: In vitro culture of VMH astrocytes of DIO and DR females with 1 day, 3 days or 4 days of FA treatment

4.2.1 Measures of cytokine production

In this experiment, we investigated the effect of specific fatty acid exposure on VMH astrocyte cytokine production in chow diet-fed DIO and DR rats. Here we considered IL-6, IL-1β and TNF-α as inflammatory cytokines (Tha et al. 2000, Wang et al. 2015). An increase in their concentration after a given treatment (compared to the vehicle group) will be interpreted as a pro-inflammatory effect. Our results showed that the production of inflammatory cytokines was already increased after 24h from the first treatment (**Fig. 4 and 5**). Indeed, in DR astrocytes, OA decreased IL-6 concentration ($P< 0.01$, **Fig 4B**) while LA increased TNF-α (**Fig. 4F**) compared to vehicle. In DIO astrocytes, OA and LA decreased the concentration of all three cytokines. Thus, LA exerted an opposite effect in DIO and DR astrocytes with the cytokine release being increased in DR and decreased in DIO.

Overall, PA and SA induced a pro-inflammatory effect with IL-6, IL-1β and TNF-α concentration being increased compared to vehicle in both DR and DIO astrocytes. Considering the concentration of cytokines 24h after the first treatment expressed as percent of vehicle, DR-PA treated astrocytes showed higher levels of IL-1β and TNF-α compared to DIO-PA treated ones.

Thus, the treatment of astrocytes revealed a beneficial effect of unsaturated FA by lowering the concentration of inflammatory cytokines compared to saturated FA (**Fig. 4 and 5**). Finally, DR rats' astrocytes presented higher cytokines levels 24 hours after unsaturated and saturated FA treatment compared to DIO rats (**Fig. 4 and 5)**, with the exception of IL-6 in response to saturated FA treatment. Cytokine levels remained similar after 72h and 96h of treatment.

IL-10 and IFN-γ were also measured but their levels were almost undetectable in most groups. For this experiment we focused on DIO and DR females' astrocytes. Other analyses performed in males' ones are shown in the annex. The results obtained from the culture of DR males' astrocytes were similar to those observed in females.

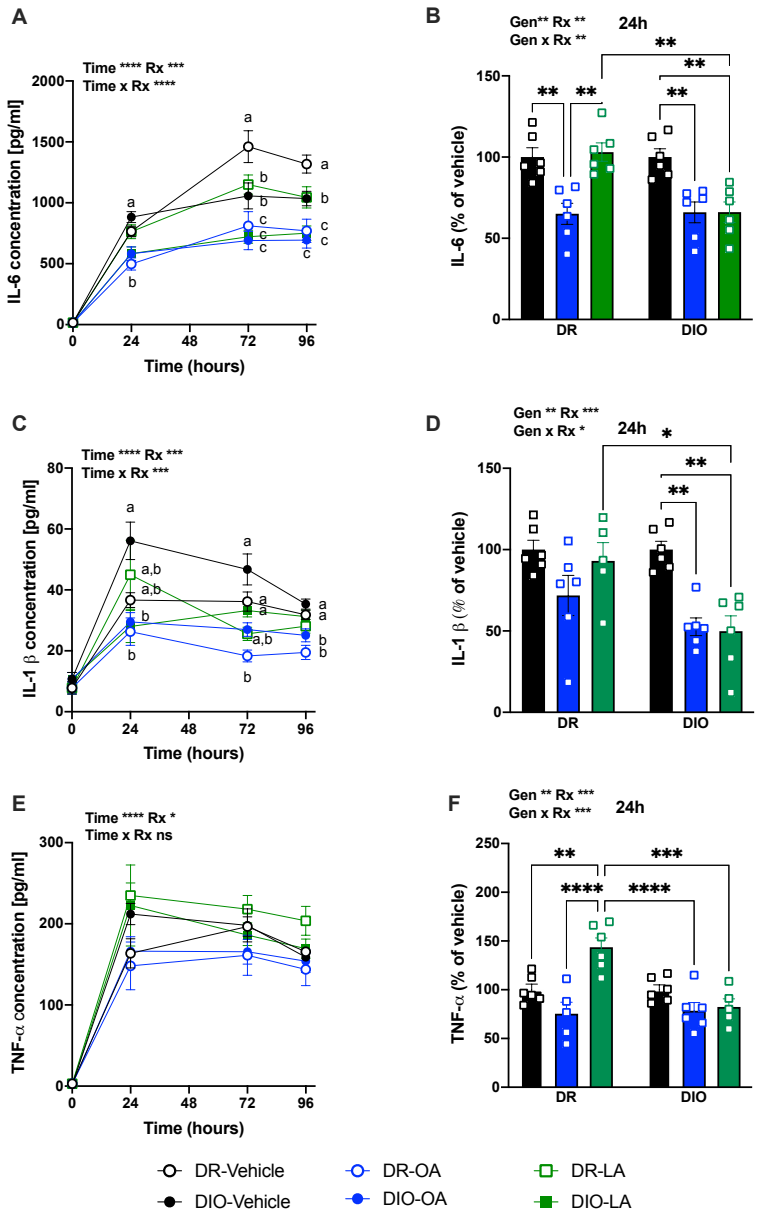

Figure 4: Effect of unsaturated fatty acid (FA) exposure on ventromedial hypothalamus (VMH) astrocyte cytokine production in chow fed DIO and DR rats. IL-6 (pg/ml) (A, B), IL-1β (pg/ml) (C, D) and TNF-α (pg/ml) (E, F) concentration in media harvested from the culture of female DIO and DR astrocytes that were treated for 96 hours with either 13 µM oleic (OA) or linoleic acid (LA) (or the same volume of media in the vehicle treated group) (A, C, E). B; D; F: concentration of cytokines 24h after the first treatment expressed as percent of vehicle. All data are expressed as mean ± SEM; n = 5-6/group. Statistics: ns > 0.05; *P ≤ 0.05; **P≤0.01; ***P≤0.001; ****P≤0.0001 by 2-way ANOVA. (a, b, c) Data points with different superscript at each time point differ from each other by P<0.05 after multiple comparison intergroup analysis.

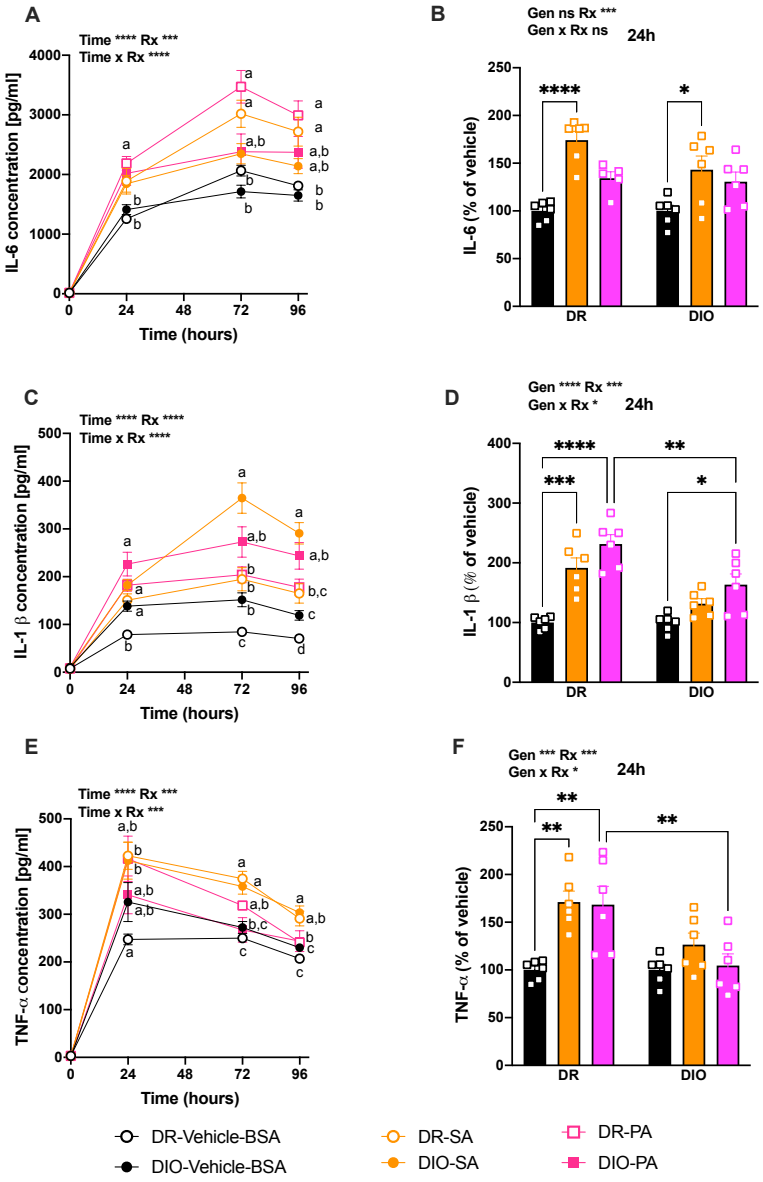

Figure 5: Effect of saturated fatty acid (FA) exposure on ventromedial hypothalamus (VMH) astrocyte cytokine production in chow fed DIO and DR rats. IL-6 (pg/ml) (A, B), IL-1β (pg/ml) (C, D) and TNF-α (pg/ml) (E, F) concentration in media harvested from the culture of female DIO and DR astrocytes that were treated for 96 hours with either 73 µM palmitic or stearic acid (or the same volume of media in the vehicle treated group) (A, C, E). B; D; F: concentration of cytokines 24h after the first treatment expressed as percent of vehicle. All data are expressed as mean ± SEM; n = 5-6/group. Statistics: ns > 0.05; *P ≤ 0.05; **P≤0.01; ***P≤0.001; ****P≤0.0001 by 2-way ANOVA. (a, b, c) Data points with different superscript at each time point differ from each other by P<0.05 after multiple comparison intergroup analysis.

4.2.2 Comparison of saturated and unsaturated FAs in relation to cytokine production

Since in the previous experiment we used different concentration of unsaturated and saturated fatty acids, we performed here an additional experiment where astrocytes of DR male rats were treated with either 10 μM oleic acid (or the same volume of media in the vehicle treated group) and 10 μM palmitic acid (or the same volume of BSA in the vehicle with BSA treated group). This additional experiment aimed to show that unsaturated FA can elicit a more potent anti-inflammatory response compared to saturated ones even at the same concentration. Our results confirmed our hypothesis, indeed the cytokine concentration was higher in astrocytes treated with 10 μM PA than in those treated with 10 μM OA (**Fig. 6**). This effect reached statistical significance for IL-1β ($P<0.05$, **Fig. 6E**)

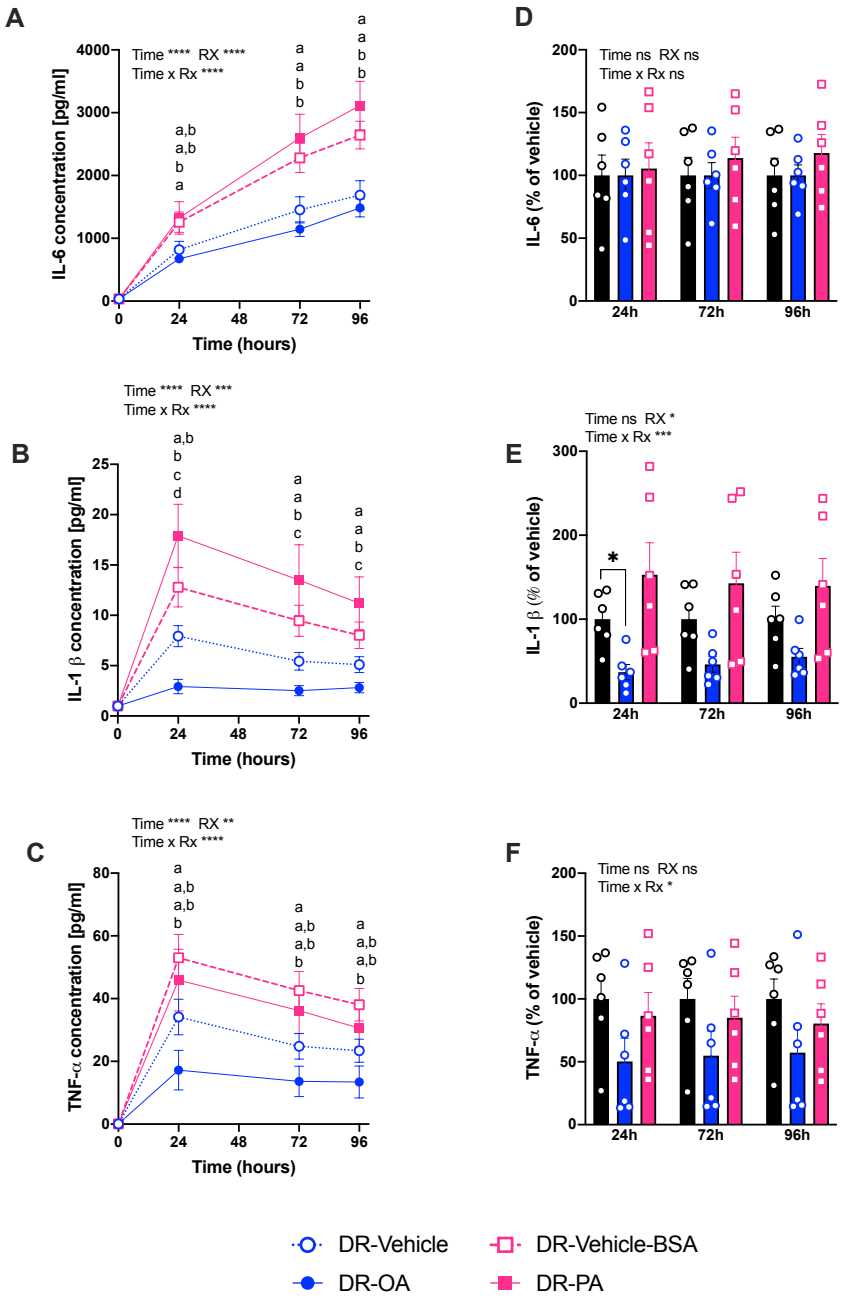

Figure 6: Effect of PA and OA on VMH astrocyte cytokine production in chow fed DR rats. IL-6 (pg/ml) (A), IL-1β (pg/ml) (B) and TNF-α (pg/ml) (C) concentration in media harvested from the culture of male DR astrocytes that were treated for 96 hours with either 10 µM oleic or palmitic acid (or the same volume of media resp. BSA in the vehicle treated groups). IL-6 (D), IL-1β (E) and TNF-α (F) concentration expressed in percentage of vehicle in media harvested from the culture of male DR astrocytes that were treated for 96 hours with either 10 µM oleic or palmitic acid (or the same volume of media resp. BSA in the vehicle treated groups). All data are expressed as mean ± SEM; n = 6/group. Statistics: ns > 0.05; *P ≤ 0.05; **P≤0.01; ***P≤0.001; ****P≤0.0001 by 2-way ANOVA. (a, b, c, d) Data points with different superscript at each time point differ from each other by P<0.05 after multiple comparison intergroup analysis.

4.3 Experiment 3: Inhibition of inflammatory pathways in astrocytes of chow-fed DIO and DR rats

In this last experiment, we assessed the effect of inhibiting IKKβ signaling pathway in mediobasal hypothalamus astrocytes of DIO and DR rats on body weight, food intake and glucose homeostasis. The histological analysis of the brains post-sacrifice indicated that the depletion of IKKβ was unilateral and encompassed the ARC and VMN areas.

4.3.1 Body weight, body weight gain, food intake, feeding behavior and glucose tolerance

At the start of the experiment, at the age of 5 weeks, both DIO and DR rats had the same weight. After being switched to 45% HFD, DIO rats started to gain more weight compared to DR rats. Overall, DIO and DR rats body weight and body weight gain differed significantly (**Fig. 7A, B**), with DIOs being 23% heavier than DRs (**Fig. 7A**).

The depletion of IKKβ in GFAP of DIO rats (DIO IKK shRNA) decreased their body weight gain by 9% ($P = 0.06$) compared to DIO controls but it was still increased compared to DR rats (**Fig. 7B**). Food intake was also decreased in DIO IKK shRNA rats compared to DIO controls (**Fig. 7D**). In the last week of measurements, the weekly food intake of DIO IKK shRNA rats was 10.5% lower than DIO control rats (Genotype x AAV $P<0.05$).

We did not observe any difference between DR control and DR IKK shRNA rats, who exhibited similar body weight, weight gain and food intake throughout the entire study.

At 8-week-old, the rats (n=8/group) were moved in BioDAQ cages for 2 weeks in order to determine their meal patterns (food intake, meal number, meal size and meal duration). The results are presented in tables 2 and 3. No differences were observed during ad libitum feeding (**Table 1**). After a 12h fasting during the light phase followed by a refeeding at dark onset, DIO IKK shRNA rats presented the same meal pattern as DR rats: in the dark phase DIO IKK shRNA rats ate less, had smaller meals and their meal duration was decreased compared to their controls (**Table 2**).

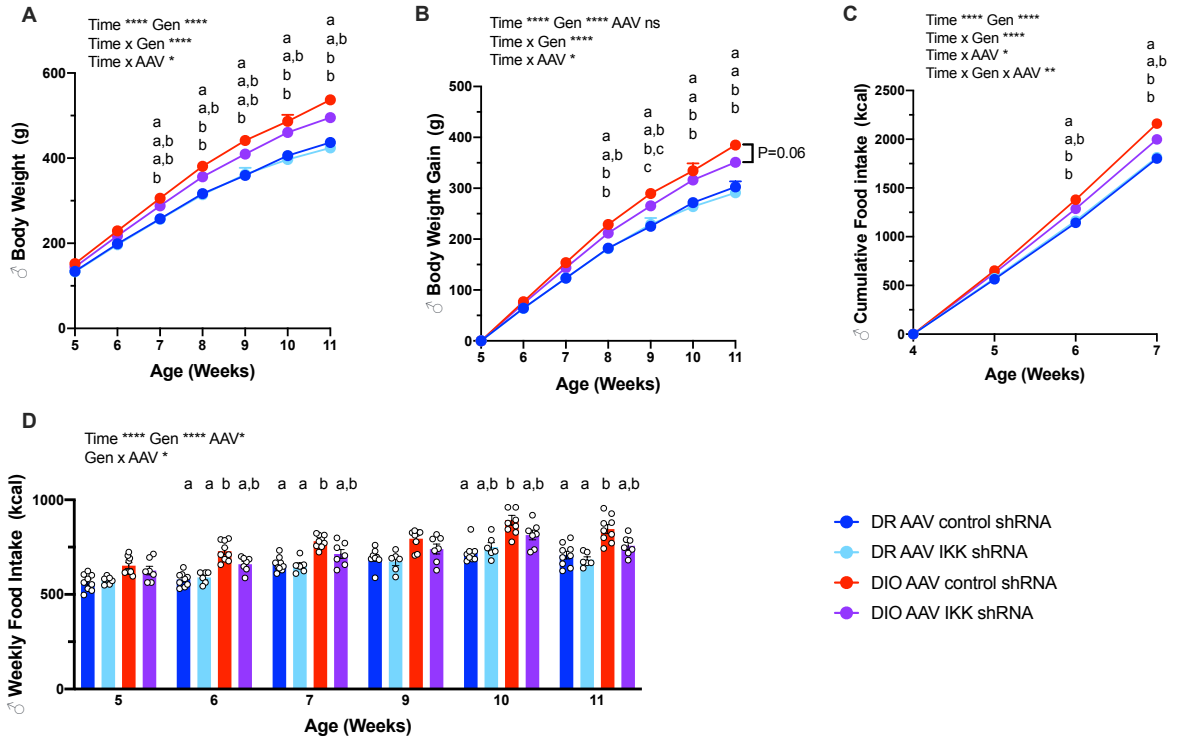

Figure 7. Body weight (A), body weight gain (B), cumulative food intake (C) and weekly food intake (D) of DIO AAV control shRNA, DR AAV control shRNA, DIO AAV IKK shRNA and DR AAV IKK shRNA male rats on high fat diet (HFD) for 7 weeks. In three DR AAV IKK shRNA rats and two DIO AAV IKK shRNA rats the AAV injection was not successful. These animals were therefore excluded from the analysis. All data are expressed as mean ± SEM; n = 6-9/group. Factors: genotype (Gen), AAV and time. Statistics: ns > 0.05; *P ≤ 0.05; **P≤0.01; ***P≤0.001; ****P≤0.0001 by 3-way ANOVA. (a, b, c) Data points with different superscript at each time point differ from each other by P<0.05 after multiple comparison intergroup analysis.

Table 1. *Ad libitum meal patterns (food intake, meal number, meal size, meal duration) during the dark phase (12 hours), the light phase (12 hours) and 24 hours of DR and DIO injected in the VMH with AAV control shRNA or AAV IKKβ shRNA*

	Dark phase (12 hours)				**Light phase (12 hours)**				**24 hours**			
	DR_AAV control	DR_AAV IKK	DIO_AAV control	DIO_AAV IKK	DR_AAV control	DR_AAV IKK	DIO_AAV control	DIO_AAV IKK	DR_AAV control	DR_AAV IKK	DIO_AAV control	DIO_AAV IKK
Total food intake (g)	19.57 ± 1.11	19.50 ± 0.87	22.97 ± 0.48	22.22 ± 1.15	1.56 ± 0.68	0.83 ± 0.29	0.51 ± 0.22	0.26 ± 0.17	21.08 ± 0.58 **a**	20.09 ± 0.73 **a**	23.32 ± 0.38 **a**	22.48 ± 1.17 **a**
Meal number	8.25 ± 0.54	8.00 ± 0.43	8.25 ± 0.57	8.08 ± 0.62	0.81 ± 0.35	0.42 ± 0.15	0.31 ± 0.13	0.17 ± 0.11	9.00 ± 0.58	8.33 ± 0.42	8.44 ± 0.65	8.25 ± 0.63
Meal size (g)	2.51 ± 0.15	2.48 ± 0.09	2.93 ± 0.24	2.92 ± 0.30	1.02 ± 0.40	1.53 ± 0.60	0.88 ± 0.41	0.52 ± 0.33	2.48 ± 0.16	2.50 ± 0.10	2.91 ± 0.25	2.89 ± 0.30
Meal duration (min)	12.12 ± 1.62	11.44 ± 1.31	12.95 ± 1.16	12.89 ± 1.99	3.26 ± 1.62	2.16 ± 0.89	1.66 ± 0.85	0.44 ± 0.44	11.90 ± 1.56	11.41 ± 1.33	12.90 ± 1.23	14.09 ± 2.00

Note. Data are expressed as mean ± SEM; n = 8/AAV control group and 6/AAV IKK group. Data are analyzed with three-way ANOVA. Factors: genotype (Gen), AAV and time. Statistics: Row 1. Time****, Gen**, Time x Gen***; Row 2. ns; Row 3. ns; Row 4. ns.

Table 2. *Meal patterns (food intake, meal number, average meal size, average meal duration) after 12-hour fasting in DR and DIO rats injected in the VMH with AAV control shRNA or AAV IKKβ shRNA*

	Dark phase (12 hours)				**Light phase (12 hours)**				**24 hours**			
	DR_AAV control	DR_AAV IKK	DIO_AAV control	DIO_AAV IKK	DR_AAV control	DR_AAV IKK	DIO_AAV control	DIO_AAV IKK	DR_AAV control	DR_AAV IKK	DIO_AAV control	DIO_AAV IKK
Total food intake (g)	21.15 ± 0.72 **a**	21.23 ± 1.16 **a**	25.42 ± 1.21 **a**	21.76 ± 0.87 **a**	0.64 ± 0.34	0	0	0.33 ± 0.33	21.79 ± 0.69	21.23 ± 1.16	25.42 ± 1.21	22.09 ± 0.90
Meal number	9.39 ± 0.53	10.00 ± 0.63	8.50 ± 0.50	9.17 ± 0.98	0.38 ± 0.18	0	0	0	9.75 ± 0.45	10.00 ± 0.63	8.50 ± 0.50	9.17 ± 0.98
Meal size (g)	2.31 ± 0.16 **a, b**	2.15 ± 0.14 **a**	3.03 ± 0.13 **b**	2.53 ± 0.31 **a, b**	1.71 ± 0.26	0	0	0	2.28 ± 0.16 **a, b**	2.15 ± 0.14 **a**	3.03 ± 0.13 **b**	2.55 ± 0.30 **a, b**
Meal duration (min)	10.87 ± 1.00 **a**	9.31 ± 1.83 **a**	15.60 ± 0.75 **a**	10.52 ± 1.42 **a**	1.29 ± 0.65	0	0	0	10.56 ± 0.89 **a**	9.31 ± 1.83 **a, b**	15.60 ± 0.75 **b**	10.71 ± 1.31 **a, b**

Note. Data are expressed as mean ± SEM; n = 8/AAV control group and 6/AAV IKK group. Data are analyzed with three-way ANOVA. Factors: genotype (Gen), AAV and time. Statistics: Row 1. Time****, Gen*, Time x Gen**, Time x Gen x AAV *; Row 2. ns; Row 3. Time****, Gen**, AAV ns; Time x Gen*, Time x AAV ns, Time x Gen x AAV*; Row 4. Time****, Gen*, AAV*, Time x Gen**, Time x AAV*, Time x Gen x AAV*.

At 10-week-old, after 5 weeks of HFD, an oral glucose tolerance test (OGTT) was performed. Baseline glucose was similar among all groups (**Fig. 8A**). A significant genotype effect was found, which indicates that DIOs are less glucose tolerant than DRs (F (1,24) = 4,364; P = 0,04). No significant effect of the AAV IKK shRNA was detected, even though DIO-depleted for IKK in GFAP displayed an overall effect indicating improved glucose tolerance curve (**Fig. 8A**).

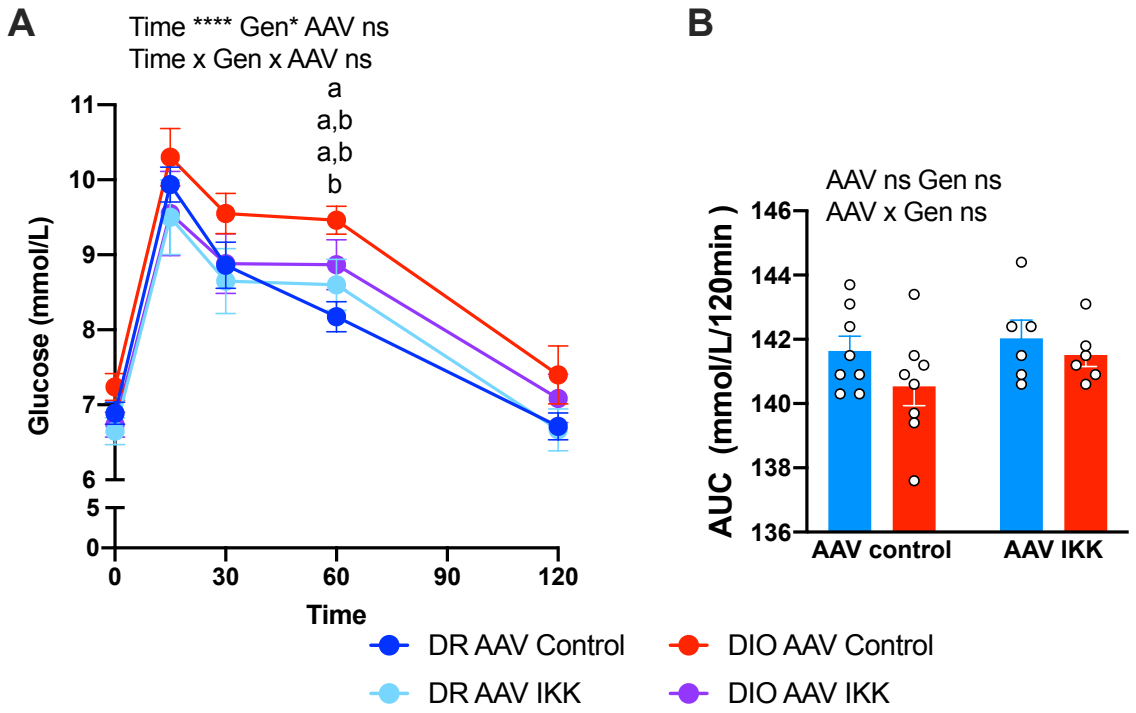

Figure 8. Oral glucose tolerance test (OGTT) in DIO AAV control shRNA, DR AAV control shRNA, DIO AAV IKK shRNA and DR AAV IKK shRNA male rats. A and B show values for the blood glucose before and 30, 60, and 120 min after the glucose load and for the area under the curve of the blood glucose during the oral glucose tolerance test (OGTT). In three DR AAV IKK shRNA rats and two DIO AAV IKK shRNA rats the AAV injection was not successful. These animals were therefore excluded from the analysis. All data are expressed as mean ± SEM; n = 6-9/group. Factors: genotype (Gen), AAV and time. Statistics: ns > 0.05; *P ≤ 0.05; **P≤0.01; ***P≤0.001; ****P≤0.0001 by 3-way ANOVA. (a, b) Data points with different superscript at each time point differ from each other by P<0.05 after multiple comparison intergroup analysis. Data in B are analyzed with two-way ANOVA.

4.3.2 Effects of inhibiting IKKβ signaling pathway in the mediobasal hypothalamus astrocytes of DIO and DR rats on energy expenditure (EE) and respiratory exchange ratio (RER)

During the last week of the study, 4 animals of each group were set-up in a TSE system to measure their EE and RER. After an acclimation period, baseline data were collected and a refeeding test was performed.

Our results showed that DIO rats displayed lower EE (**Fig 9 A, B**): a significant genotype effect was detected when EE is presented as an hourly graph (F (3,11) = 6,445; P = 0,009) or as cumulative EE (F (1,11) = 15,55; P = 0,002). Moreover, DIOs presented higher RER compared to DRs during ad libitum feeding (F (1,11) = 6,678; P = 0,025) indicating that carbohydrates were being consumed preferentially (**Fig. 9 E, F**). This outcome changed after rats were submitted to 12 hours of fasting followed by ad libitum refeeding. Indeed, during the fasting period, DIO control rats presented the lowest RER values compared to the other groups, indicative of fat oxidation (**Fig 9 G, H**). An AAV x gene interaction (in graph G (F (1,11) = 4.501; P=0.05) and H (F (1,11) = 5,246; P=0,0428)) was also observed. This result may suggest that the depletion of IKK in GFAP of DIO rats causes a switch in their metabolism.
In contrast, despite the differences found between DIO IKK rats and DIO control rats on RER values during fasting and refeeding, we found no significant effect of IKK depletion on EE. The same results were found ad libitum or after fasting and refeeding. The depletion of IKKβ had no effect on EE and RER in DR rats.

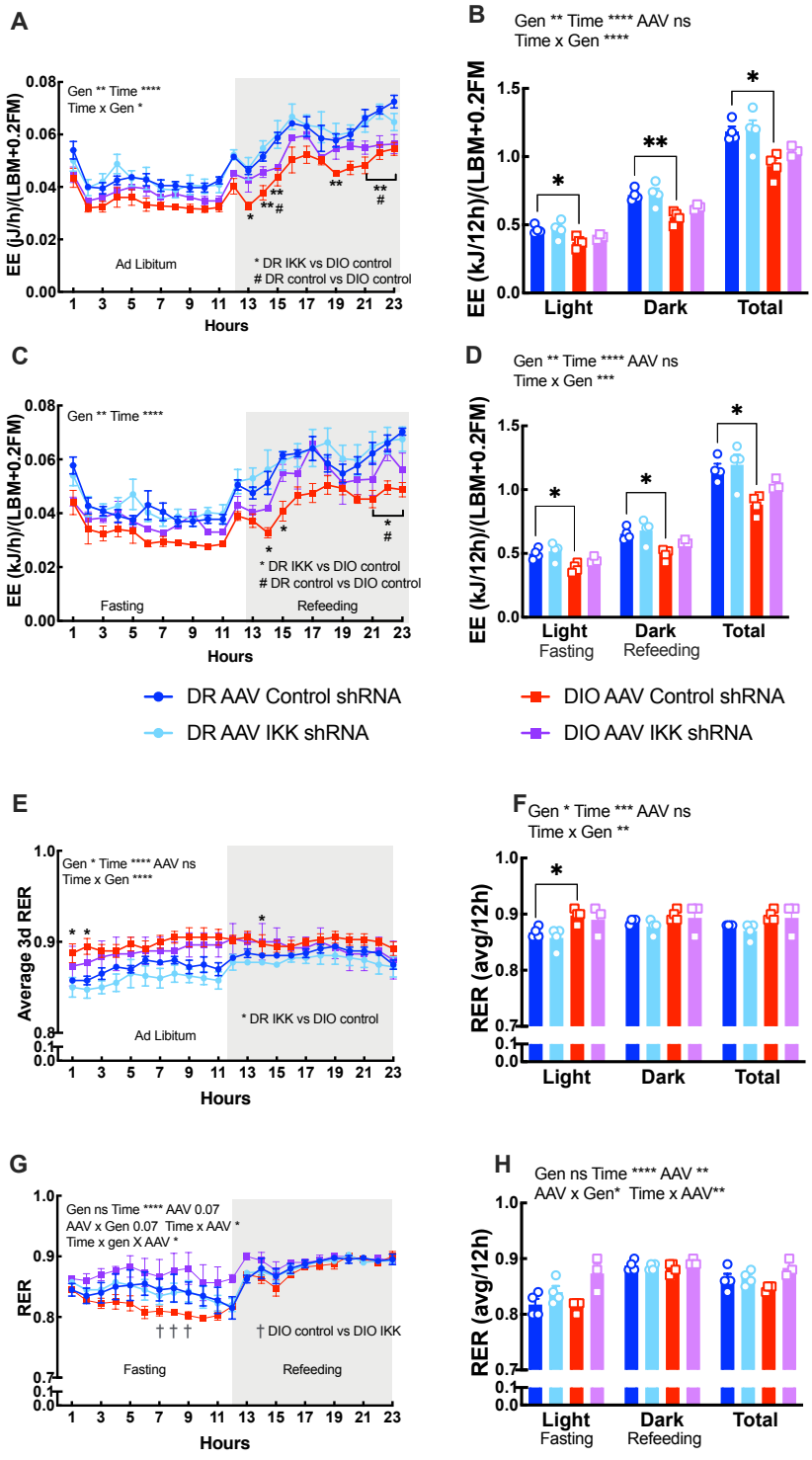

Figure 9. Energy expenditure (EE) and respiratory exchange ratio (RER) in DIO AAV control shRNA, DR AAV control shRNA, DIO AAV IKK shRNA and DR AAV IKK shRNA male rats ad libitum (A, B, E, F) and after 12 hours fasting (C, D, G, H). In one DIO AAV IKK shRNA rats the AAV injection was not successful. This animal was therefore excluded from the analysis. All data are expressed as mean ± SEM; n = 3-4/group. Factors: genotype (Gen), AAV and time. Statistics: ns > 0.05; *P ≤ 0.05; **P≤0.01; ***P≤0.001; ****P≤0.0001 by 3-way ANOVA. A, C and E: * indicates a significant difference (P<0.05) between DR AAV IKK shRNA and DIO AAV Control shRNA; # indicates a significant difference (P<0.05) between DR AAV Control shRNA and DIO AAV Control shRNA. G: † indicates a significant difference (P<0.05) between DIO AAV Control shRNA and DIOAAV IKK shRNA.

4.3.3 Body composition and plasma leptin levels on HFD of male DIO AAV IKK shRNA and DR AAV IKK shRNA rats compared to controls.

After the sacrifice, body composition analysis (EchoMRI™) was performed and the depletion of IKKβ in GFAP of DIO rats decreased the fat mass by 11.5 % compared to DIO controls (**Fig. 10A**). According to this result, DIO IKK shRNA rats also showed lower plasma leptin levels (P = 0.007) reaching comparable levels to those of DR rats (**Fig. 10B**). Together with the decreased RER, this suggests a role of astrocytes inflammatory pathway in the repartition of lipid storage and utilization. The LBM + 0.2 FM values were used to normalize EE and RER obtained from the TSE system.

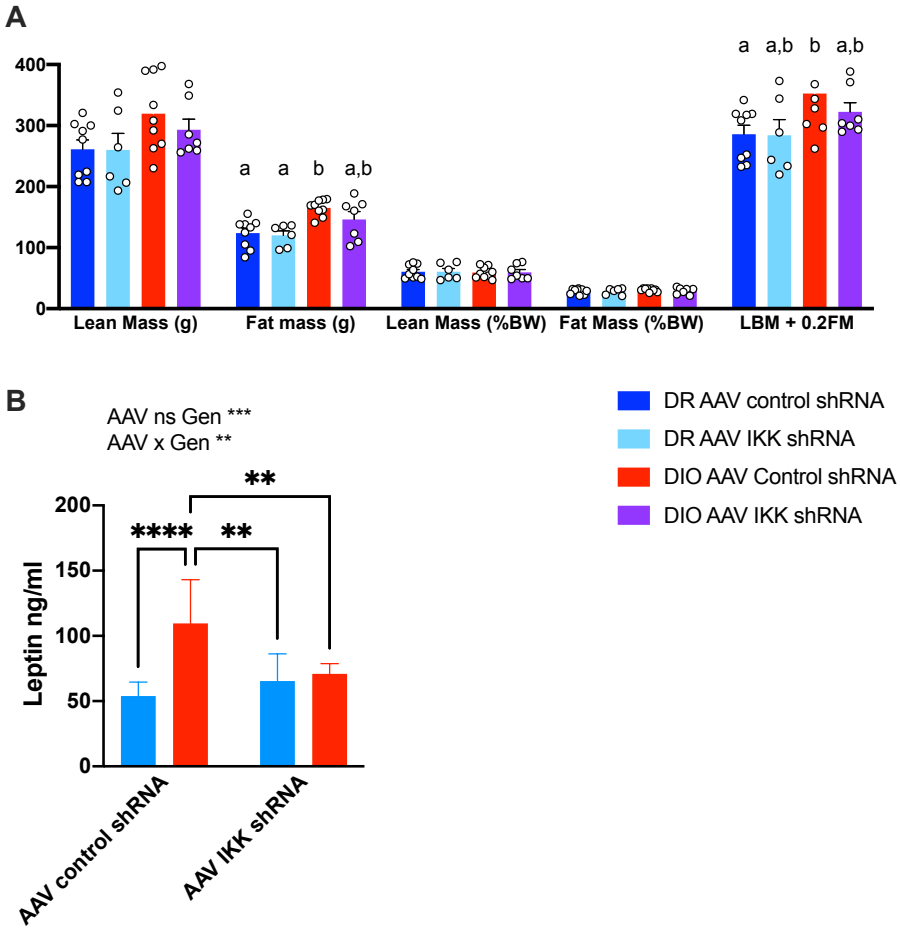

Figure 10. Body composition (A) and plasma leptin concentration (B) of DIO AAV control shRNA, DR AAV control shRNA, DIO AAV IKK shRNA and DR AAV IKK shRNA male rats after 7 weeks of HFD. In three DR AAV IKK shRNA rats and two DIO AAV IKK shRNA rats the AAV injection was not successful. These animals were therefore excluded from the analysis. All data are expressed as mean ± SEM; n = 6-9/group. Factors: genotype (Gen), AAV and time. Statistics: ns > 0.05; *P ≤ 0.05; **P≤0.01; ***P≤0.001; ****P≤0.0001 by 3-way ANOVA. (a, b) Data points with different superscript at each time point differ from each other by P<0.05 after multiple comparison intergroup analysis. Data in B are analyzed with two-way ANOVA.

4.3.4 Immunohistochemistry (IHC) and qPCR to validate AAV GFAP-IKKβ shRNA transfection

We used two animals per group to show the efficacy of the AAV GFAP-IKKβ shRNA virus. After harvesting brain tissues from the ARC, VMN, and hypothalamic dorsomedial nucleus (DMN), the depletion of IKK against the housekeeping gene GAPDH was measured by qPCR. Our results showed that on the injected side, the depletion was 60% in DR AAV IKK rats and 66% in DIO AAV IKK (**Fig. 11C**). In addition, the co-localization of GFAP and AAV is shown Fig. 11A and B.

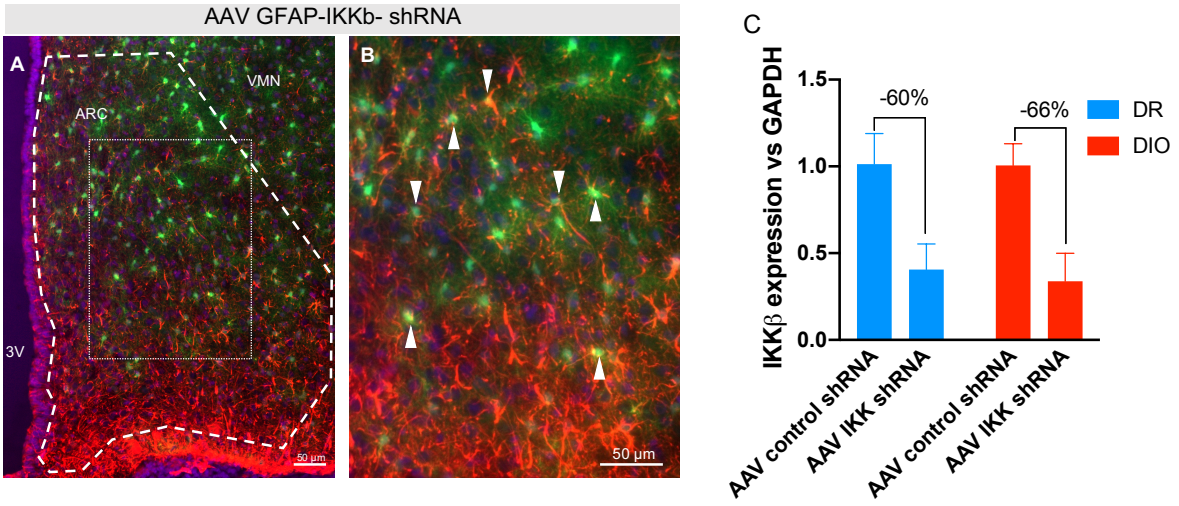

Figure 11. Validation of the virus model. A. Representative 20X image of a AAV injection of AAV GFAP-IKKβ shRNA virus (green) in the medio basal hypothalamus of an adult DIO rat colocalized with astrocytes (red). B. Representative 40X image of the boxed area in A; colocalization of GFAP staining and AAV GFAP-IKKβ shRNA indicated by white arrows. C. IKKβ expression vs. the housekeeping gene GAPDH in DIO AAV control shRNA, DR AAV control shRNA, DIO AAV IKK shRNA and DR AAV IKK shRNA male rats.

5. Discussion

The first aim of this study was to determine the effect of an acute high energy diet (HE) exposure on glial activation and cytokine production in DIO and DR rats and to assess whether sex-differences influence glial inflammation. Second, we aimed to investigate the effect of inhibiting the IKKβ signaling pathway, a key inflammatory pathway mediator, in mediobasal hypothalamus' astrocytes of DIO and DR rats on metabolism.

Our results showed that after 3 days of HE diet, DIO and DR rats ate and gained more weight compared to rats fed chow diet. On day 2 and 3 of HE diet, DR rats were able to reduce their caloric intake compared to DIO rats. In addition, DR rats who consumed a HE diet for 4 weeks showed similar plasma leptin levels to chow, 3d HE or 3d pair-fed rats. This was not the case for DIO rats, who displayed higher levels of plasma leptin already after 3d of HE diet, which is consistent with their obese status.
Further, we provided evidence that VMH astrocyte cytokine production is increased already 24 hours after the exposure to LCFA in vitro and that unsaturated FA can elicit a more potent anti-inflammatory response compared to saturated FA which have instead a pro-inflammatory effect.
The depletion of IKKβ in astrocytes of DIO rats fed 45% HFD for 7 weeks partially prevented weight gain and produced meal pattern similar to that of DR rats. DIO IKK shRNA rats had less fat mass and drastically lower leptin plasma levels compared to DIO control rats. Both parameters reached comparable levels to those of DR rats.

5.1. 3d of HE diet does not affect the ARC density of GFAP astrocyte and Iba-1 microglia in DIO and DR rats

We did not observe a significant difference in GFAP and Iba-1 density between male and female DIO-DR rats fed chow or HE diet. This is in contrast with previous data of our research group, which showed that on chow diet, GFAP was increased while Iba1 was decreased in DIO rats compared to DR rats (Janine Schläpfer Master Thesis, VSF). This difference could be due to the different generation used between the two studies (F3 vs. F5) and/or to the animals' age at the time of the sacrifice. Indeed, F3 animals were maintained on chow for 4 weeks longer than the F5 generation. Indeed, aged animals appear to be more susceptible to develop HFD-induced neuroinflammation (Spencer et al. 2019). Hsu et al. (2015) also observed age-

dependent inflammation effects of exposure to sugar-rich diets. These studies remind us of the importance of considering the age of the animal at the time of the experiment, as it can play an important role in the outcome. Nevertheless, even though astrocyte and microglia density remain unchanged after 3d of HE, we could still hypothesize that hypothalamic cytokines would be elevated after 3 days of HE diet. Indeed, Cansell et al. (2020) showed that post prandial hypothalamic inflammation is a process that occur already in the first hours after HFD exposure, prior to reactive gliosis in the ARC.

We must also consider the different types of diets used (HE vs. 45% HFD). Both have a similar amount of calories per gram. However, the HFD diet has a higher fat content (45% vs. 15.6% for HE), but less carbohydrates (35% vs. 56.7% for HE). Thus, the macronutrient composition of the diets can be a major factor when assessing hypothalamic inflammation, with fatty acids being more detrimental than high amounts of sugar.

In this study, we only measured cell density. The increase in cell body size is the last stage of gliosis (Schiweck et al. 2018). Further measurements could next be conducted to investigate in more detail cell morphology. Early brain inflammation is characterized by an increase in the number of branches and the length of cellular processes in astrocytes and microglial cells (Harrison et al. 2019). The measure of these parameters might have helped to uncover whether reactive gliosis take places after 3d of HE diet. To further confirm the cellular activation of Iba-1 and GFAP positive cells, the measure of pJNK, a marker of inflammation, may also be helpful (Benzler et al. 2015).

5.2 Pro- and anti-inflammatory effect of FA on primary astrocytes

In the second part of our study we investigated the effect of LCFA on primary culture of DIO and DR VMH astrocytes. To my knowledge, this is the first time that inflammatory cytokine production has been quantified in media harvested from LCFA-treated primary hypothalamic astrocytes. Overall, unsaturated FA presented anti-inflammatory properties while saturated FA were pro-inflammatory (Milanski et al. 2009).

Interestingly, primary astrocytes harvested from DR rats secreted more inflammatory cytokines than DIO. This finding was particularly evident after the treatment with linoleic acid. One possible explanation could be that these cytokines are protective after a short exposure to FA or may trigger a satiety signal. Indeed, it has been shown that cytokines such as IL-6 can trigger

meal termination (Timper et al. 2017). Our experiment can also be compared to the in vivo experiments performed by Cansell et al. where they showed that after one meal IL1-β, IL-6 and TNF-α are increased.

Nevertheless, our results do not agree with our working hypothesis that DIO rats ARC cells produce more inflammatory cytokines that will predispose the animals to developing obesity. To explain this discrepancy we could hypothesize that we isolated astrocytes from 3-week-old chow-fed DIO and DR rats; at that age, DIO rats were not yet obese. To increase their obese phenotype, we could expose the rats to HE diet before weaning, and this may perhaps also alter astrocyte cytokine secretion. Indeed, Le Foll et al. (2009) reported that DIO rats exposed to HE diet before weaning showed worsening of FA neuronal sensing alterations compared to chow diet. Such altered sensitivities may underlie the propensity of DIO offspring to become obese when fed high-fat, high-sucrose diets.

5.3 Inhibition of IKKβ/NF-kB signaling in astrocytes partially prevent DIO rats to become obese

First, we were able to show that the depletion of IKKβ was around 60% in DR AAV IKK rats and 66% in DIO AAV IKK. These numbers can be judged as satisfactory considering that the analyzed tissue also contained other cell types, such as neurons and microglia, in which IKKβ was not inhibited. The specificity of the depletion was then confirmed by co-labelling with GFAP.

The depletion of IKKβ in DR astrocytes did not elicit any significant effects. On the other hand, it led to multiple behavioral alterations in DIO rats. We previously discussed the defective VMH neuronal FA and KB sensing of DIO rats (Le Foll et al. 2015b) and we had hypothesized that hypothalamic inflammation could contribute to these alterations. HFD induces astrocyte and microglia activation associated with low grade inflammation in mice and rats (Thaler et al. 2010, Arruda et al. 2011, Garcia-Caceres et al. 2013). Therefore, it is possible that the increase in FI seen during a chronic HFD feeding regimen in DIO rats could be due to the action of inflammatory cytokines on neuronal FA sensing. In that case, our attempt to reduce hypothalamic inflammation via inhibition of the IKKβ pathway may have a positive effect, leading to improved control of hunger and weight gain in DIO rats. We can postulate that IKKβ depletion may restore neuronal KB sensing in DIO-fed HFD and prevent obesity.

DIO meal patterns have undergone significant changes after the fasting refeeding test with the meal pattern of DIO IKK-depleted rats being similar to those of DR rats. During fasting, it has been shown that tanycytes, which are glial cells located along the 3rd ventricle, facilitate the entry of circulating hormones and nutrients into the hypothalamus with the purpose of controlling refeeding hyperphagia (Douglass et al. 2016). We can thus hypothesize that the hormone and nutrient increase within the VMH may explain why the meal pattern of DIO IKK-depleted rats are normalized once the animals are subjected to a fasting-refeeding test.

In general, our results confirmed the characteristics that distinguish DIO from DR rats and provide evidence toward lesser-known characteristics. To be more specific, DIO rats on 45% HFD presented lower EE compared to DR rats. Indeed, it is known that a diet rich in fat can negatively affect EE (Frihauf et al. 2016). The lower energy consumption of DIO rats in addition to their tendency to consume more food can here be considered as a key characteristic that distinguishes them from DR rats and contributes to their obese phenotype. DIO rats showed higher RER values compared with DRs during ad libitum feeding, suggesting that carbohydrates were metabolized preferentially. During the 12-h of fasting, DIO control rats decreased their RER, whereas DIO-IKK rats showed the highest values among all groups. One possible explanation is that during a fasting phase, fat mass is directly correlated with RER. Consistent with this hypothesis, DIO control rats, which had more fat mass compared with DIO-IKK rats, consumed more fat than carbohydrate during fasting. Our results clearly showed a benefit of IKKβ depletion in lowering plasma leptin levels in DIO rats. This effect could be due to a decrease in subcutaneous fat but not in visceral fat pad since leptin is mainly released from subcutaneous fat (Masuzaki et al. 1995). Because we did not perform fat pad-specific analysis, this claim cannot be confirmed.

Our results are consistent with some previous studies performed in mice. Benzler et al. (2015) found that the non-cell specific inhibition of IKKβ/NF-kB signaling attenuated HFD-induced body weight gain and body fat mass accumulation as well as a decrease in EE. Douglas et al. (2017) showed that temporal depletion of IKKβ in GFAP-cre ERT2 mice after 6 weeks of HFD feeding prevented glucose intolerance and protected the mice from further weight gain. However when IKKβ knock-out was performed in chow-fed GFAP-Cre ERT2 mice which were then put on 60% HFD, no effect of the depletion on behavior was observed. Since DIO rats are predisposed to becoming obese, opposite to GFAP-cre ERT2 mice, we were able to prevent the

development of obesity even if they were not preloaded with HFD before the GFAP-IKKβ knocked-down. Another study assessing astrocytes inflammatory pathways (Buckman et al. (2014)) found that the inhibition of NF-kB signaling in astrocytes was effective in preventing acute HFD-induced astrocyte activation. Taken together, these results claim the NF-kB/IKKβ pathway to be an important signal required for diet-induced obesity.

To further confirm the role of cytokines in mediating the development of the DIO phenotype, we will next measure the cytokine secretion in mediobasal hypothalamic tissues; and to test whether the activation of the IKKβ pathway is decreased after depletion, co-labelling with pJNK will be performed in ARC brain sections.

Finally, while these results are of importance, the improved neuronal response after IKKβ inhibition remain to be tested.

5.4 Outlook and limitations of the IKKβ study

Unfortunately even though the rats were bilaterally injected in the ARC/VMN with previously validated coordinates (Le Foll et al. 2015a), the histological analysis revealed that the virus was present only on one side. We hypothesized that the distance between the two lateral injections were too narrow and not deep enough for such young rats. To be more accurate and in order to target exclusively the ARC, we will next use a greater dorso-ventral coordinate. In detail, the new coordinates that we suggest and that need to be further demonstrated are: 2.6 mm posterior, ±0.4 mm lateral, and 8.7 mm ventral from the bregma (the latter relative to the dura mater). Important, even after a unilateral injection we can already observe an improvement of the DIO phenotype, we thus expect an even greater improvement after successful bilateral injections.

6. References

Arruda, A.P., et al., Low-grade hypothalamic inflammation leads to defective thermogenesis, insulin resistance, and impaired insulin secretion. Endocrinology, 2011. 152(4): p. 1314-26

Ávalos Y, Kerr B, Maliqueo M, Dorfman M. Cell and molecular mechanisms behind diet-induced hypothalamic inflammation and obesity. J Neuroendocrinol. 2018 Oct;30(10):e12598. doi: 10.1111/jne.12598. Epub 2018 Aug 7. PMID: 29645315.

Benarroch EE. Glycogen metabolism: metabolic coupling between astrocytes and neurons. Neurology. 2010 Mar 16;74(11):919-23. Doi: 10.1212/WNL. 0b013e3181d3e44b. PMID: 20231669.

Benzler J, Ganjam GK, Pretz D, Oelkrug R, Koch CE, Legler K, Stöhr S, Culmsee C, Williams LM, Tups A. Central inhibition of IKKβ/NF-κB signaling attenuates high-fat diet-induced obesity and glucose intolerance. Diabetes. 2015 Jun;64(6):2015-27. doi: 10.2337/db14-0093. Epub 2015 Jan 27. PMID: 25626735.

Bouchard, C. and A. Tremblay, Genetic influences on the response of body fat and fat distribution to positive and negative energy balances in human identical twins. J.Nutr., 1997. 127: p. 943S-947S.

Buckman LB, Thompson MM, Lippert RN, Blackwell TS, Yull FE, Ellacott KL. Evidence for a novel functional role of astrocytes in the acute homeostatic response to high-fat diet intake in mice. Mol Metab. 2014 Oct 16;4(1):58-63. doi: 10.1016/j.molmet.2014.10.001. PMID: 25685690; PMCID: PMC4314532.

Cansell, C, Stobbe, K, Sanchez, C, et al. Dietary fat exacerbates postprandial hypothalamic inflammation involving glial fibrillary acidic protein-positive cells and microglia in male mice. *Glia*. 2020; 69: 42– 60.

Débora G. Souza, Roberto F. Almeida, Diogo O. Souza, Eduardo R. Zimmer, The astrocyte biochemistry, Seminars in Cell & Developmental Biology, Volume 95, 2019, Pages 142-150, ISSN 1084-9521.

Dong, Y. and Benveniste, E.N. (2001), Immune function of astrocytes. Glia, 36: 180-190.

Dorfman, M. D., & Thaler, J. P. (2015). Hypothalamic inflammation and gliosis in obesity. Current Opinion in Endocrinology, Diabetes and Obesity, Vol. 22, pp. 325–330.

Douglass JD, Dorfman MD, Thaler JP. Glia: silent partners in energy homeostasis and obesity pathogenesis. Diabetologia. 2017 Feb;60(2):226-236. doi: 10.1007/s00125-016-4181-3. Epub 2016 Dec 16. PMID: 27986987; PMCID: PMC5253392.

Douglass JD, Dorfman MD, Fasnacht R, Shaffer LD, Thaler JP. Astrocyte IKKβ/NF-κB signaling is required for diet-induced obesity and hypothalamic inflammation. Mol Metab. 2017 Jan 28;6(4):366-373. doi: 10.1016/j.molmet.2017.01.010. PMID: 28377875; PMCID: PMC5369266.

Duffy S, Lutz TA, Boyle CN. Rodent models of leptin receptor deficiency are less sensitive to amylin. Am J Physiol Regul Integr Comp Physiol. 2018 Oct 1;315(4):R856-R865. doi: 10.1152/ajpregu.00179.2018. Epub 2018 Aug 22. PMID: 30133304.

Even PC, Nadkarni NA. Indirect calorimetry in laboratory mice and rats: principles, practical considerations, interpretation and perspectives. Am J Physiol Regul Integr Comp Physiol. 2012 Sep 1;303(5):R459-76. doi: 10.1152/ajpregu.00137.2012. Epub 2012 Jun 20. Erratum in: Am J Physiol Regul Integr Comp Physiol. 2015 Dec 1;309(11):R1460. PMID: 22718809.

Ferrario CR, Labouèbe G, Liu S, Nieh EH, Routh VH, Xu S, O'Connor EC. Homeostasis Meets Motivation in the Battle to Control Food Intake. J Neurosci. 2016 Nov 9;36(45):11469-11481. doi: 10.1523/JNEUROSCI.2338-16.2016. PMID: 27911750; PMCID: PMC5125214.

Frihauf JB, Fekete ÉM, Nagy TR, Levin BE, Zorrilla EP. Maternal Western diet increases adiposity even in male offspring of obesity-resistant rat dams: early endocrine risk markers. Am J Physiol Regul Integr Comp Physiol. 2016 Dec 1;311(6):R1045-R1059. doi: 10.1152/ajpregu.00023.2016. Epub 2016 Sep 21. PMID: 27654396; PMCID: PMC5256983.

Garcia-Caceres, C., C.X. Yi, and M.H. Tschop, Hypothalamic astrocytes in obesity. Endocrinol Metab Clin North Am, 2013. 42(1): p. 57-66.

Giuliani C, Napolitano G, Bucci I, Montani V, Monaco F. [Nf-kB transcription factor: role in the pathogenesis of inflammatory, autoimmune, and neoplastic diseases and therapy implications] La Clinica Terapeutica. 2001 Jul-Aug;152(4):249-253.

Gorina R, Font-Nieves M, Márquez-Kisinousky L, Santalucia T, Planas AM. Astrocyte TLR4 activation induces a proinflammatory environment through the interplay between MyD88-dependent NFκB signaling, MAPK, and Jak1/Stat1 pathways. Glia. 2011 Feb;59(2):242-55. doi: 10.1002/glia.21094. PMID: 21125645.

Harrison L, Pfuhlmann K, Schriever SC, Pfluger PT. Profound weight loss induces reactive astrogliosis in the arcuate nucleus of obese mice. Mol Metab. 2019 Jun;24:149-155. doi: 10.1016/j.molmet.2019.03.009. Epub 2019 Apr 3. PMID: 30979678; PMCID: PMC6977167.

Ilia D. Vainchtein, Anna V. Molofsky, Astrocytes and Microglia: In Sickness and in Health, Trends in Neurosciences, Volume 43, Issue 3, 2020, Pages 144-154, ISSN 0166-2236.

Kim JD, Yoon NA, Jin S, Diano S. Microglial UCP2 Mediates Inflammation and Obesity Induced by High-Fat Feeding. Cell Metab. 2019 Nov 5;30(5):952-962.e5. doi: 10.1016/j.cmet.2019.08.010. Epub 2019 Sep 5. PMID: 31495690; PMCID: PMC7251564.

Le Foll C, Irani BG, Magnan C, Dunn-Meynell A, Levin BE. Effects of maternal genotype and diet on offspring glucose and fatty acid-sensing ventromedial hypothalamic nucleus neurons. Am J Physiol Regul Integr Comp Physiol. 2009 Nov;297(5):R1351-7. doi: 10.1152/ajpregu.00370.2009. Epub 2009 Aug 26. PMID: 19710389; PMCID: PMC2777766.

Le Foll C, Dunn-Meynell AA, Levin BE. Role of FAT/CD36 in fatty acid sensing, energy, and glucose homeostasis regulation in DIO and DR rats. Am J Physiol Regul Integr Comp Physiol. 2015 (a) Feb 1;308(3):R188-98. doi: 10.1152/ajpregu.00367.2014. Epub 2014 Dec 4. PMID: 25477422; PMCID: PMC4313072

Le Foll C, Dunn-Meynell AA, Miziorko HM, Levin BE. Role of VMH ketone bodies in adjusting caloric intake to increased dietary fat content in DIO and DR rats. Am J Physiol Regul Integr Comp Physiol. 2015 (b) May 15;308(10):R872-8. doi: 10.1152/ajpregu.00015.2015. Epub 2015 Mar 18. PMID: 25786485; PMCID: PMC4436979.

Le Foll C, Johnson MD, Dunn-Meynell AA, Boyle CN, Lutz TA, Levin BE. Amylin-Induced Central IL-6 Production Enhances Ventromedial Hypothalamic Leptin Signaling. *Diabetes*. 2015 (c) ;64(5):1621. doi:10.2337/db14-0645

Le Foll C, Levin BE. Fatty acid-induced astrocyte ketone production and the control of food intake. Am J Physiol Regul Integr Comp Physiol. 2016 Jun 1;310(11):R1186-92. doi: 10.1152/ajpregu.00113.2016. Epub 2016 Apr 27. PMID: 27122369; PMCID: PMC4935491.

Lee JA, Hall B, Allsop J, Alqarni R, Allen SP. Lipid metabolism in astrocytic structure and function. Semin Cell Dev Biol. 2020 Aug 6:S1084-9521(19)30257-5. doi: 10.1016/j.semcdb.2020.07.017. Epub ahead of print. PMID: 32773177.

Levin, B.E., J. Triscari, and A.C. Sullivan, Metabolic features of diet-induced obesity without hyperphagia in young rats. Am.J.Physiol., 1986. 251: p. R433-R440.

Levin, B.E. and A.A. Dunn-Meynell, Reduced central leptin sensitivity in rats with diet-induced obesity. Am J Physiol Regul Integr Comp Physiol, 2002. 283(4): p. R941-8.

Levin, B.E., et al., A new obesity-prone, glucose-intolerant rat strain (F.DIO). Am J Physiol Regul Integr Comp Physiol, 2003 (a). 285(5): p. R1184-91.

Levin B.E., Dunn-Meynell AA, Ricci MR, Cummings DE. Abnormalities of leptin and ghrelin regulation in obesity-prone juvenile rats. Am J Physiol Endocrinol Metab. 2003 Nov;285(5):E949-57. doi: 10.1152/ajpendo.00186.2003. Epub 2003 (b). PMID: 12865257.

Levin, B.E., Christophe Magnan, Ambrose Dunn-Meynell, Christelle Le Foll, Metabolic Sensing and the Brain: Who, What, Where, and How?, *Endocrinology*, Volume 152, Issue 7, 1 July 2011, Pages 2552–2557.

Masuzaki H, Ogawa Y, Isse N, Satoh N, Okazaki T, Shigemoto M, Mori K, Tamura N, Hosoda K, Yoshimasa Y, et al. Human obese gene expression. Adipocyte-specific expression and regional differences in the adipose tissue. Diabetes. 1995 Jul;44(7):855-8. doi: 10.2337/diab.44.7.855. PMID: 7789654.

Michael W Schwartz, Randy J Seeley, Lori M Zeltser, Adam Drewnowski, Eric Ravussin, Leanne M Redman, Rudolph L Leibel, Obesity Pathogenesis: An Endocrine Society Scientific Statement, *Endocrine Reviews*, Volume 38, Issue 4, 1 August 2017, Pages 267–296.

Milanski M, Degasperi G, Coope A, et al. Saturated fatty acids produce an inflammatory response predominantly through the activation of TLR4 signaling in hypothalamus: implications for the pathogenesis of obesity. *J Neurosci*. 2009;29(2):359-370. doi:10.1523/JNEUROSCI.2760-08.2009

Nathalia R. Dragano, Milena Monfort-Pires, Licio A. Velloso, Mechanisms Mediating the Actions of Fatty Acids in the Hypothalamus, Neuroscience, Volume 447, 2020, Pages 15-27, ISSN 0306-4522.

Obici S, Feng Z, Morgan K, Stein D, Karkanias G, Rossetti L. Central administration of oleic acid inhibits glucose production and food intake. Diabetes 51: 271–275, 2002.

Obici S, Feng Z, Arduini A, Conti R, Rossetti L. Inhibition of hypothalamic carnitine palmitoyltransferase-1 decreases food intake and glucose production. Nat Med 9: 756–761, 2003.

Piattini F, Le Foll C, Kisielow J, Rosenwald E, Nielsen P, Lutz T, Schneider C, Kopf M. A spontaneous leptin receptor point mutation causes obesity and differentially affects leptin signaling in hypothalamic nuclei resulting in metabolic dysfunctions distinct from db/db mice. Mol Metab. 2019 Jul;25:131-141. doi: 10.1016/j.molmet.2019.04.010. Epub 2019 Apr 25. PMID: 31076350; PMCID: PMC6601129.

Ricci, M.R. and B.E. Levin, Ontogeny of diet-induced obesity in selectively-bred Sprague-Dawley rats. Am.J.Physiol., 2003. 285: p. R610-R618.

Schiweck J, Eickholt BJ, Murk K. Important Shapeshifter: Mechanisms Allowing Astrocytes to Respond to the Changing Nervous System During Development, Injury and Disease. Front Cell Neurosci. 2018 Aug 21;12:261. doi: 10.3389/fncel.2018.00261. PMID: 30186118; PMCID: PMC6111612.

Seong J, Kang JY, Sun JS, Kim KW. Hypothalamic inflammation and obesity: a mechanistic review. Arch Pharm Res. 2019 May;42(5):383-392. doi: 10.1007/s12272-019-01138-9. Epub 2019 Mar 5. PMID: 30835074.

Stunkard, A.J., Genetic contributions to human obesity. Res Publ Assoc Res Nerv Ment Dis, 1991. 69: p. 205-18.

Swamini P. Sinha, Pelin Avcu, Kevin M. Spiegler, Sreeya Komaravolu, Kevin Kim, Tara Cominski, Richard J. Servatius, Kevin C.H. Pang, Startle suppression after mild traumatic brain injury is associated with an increase in pro-inflammatory cytokines, reactive gliosis and neuronal loss in the caudal pontine reticular nucleus, Brain, Behavior, and Immunity, Volume 61, 2017, Pages 353-364, ISSN 0889-1591.

Tha KK, Okuma Y, Miyazaki H, Murayama T, Uehara T, Hatakeyama R, Hayashi Y, Nomura Y. Changes in expressions of proinflammatory cytokines IL-1beta, TNF-alpha and IL-6 in the brain of senescence accelerated mouse (SAM) P8. Brain Res. 2000 Dec 1;885(1):25-31. doi: 10.1016/s0006-8993(00)02883-3. PMID: 11121526.

Thaler, J.P., et al., Hypothalamic inflammation and energy homeostasis: resolving the paradox. Frontiers in neuroendocrinology, 2010. 31(1): p. 79-84.

Thaler, J.P., Yi C-X, Schur EA, et al. Obesity is associated with hypothalamic injury in rodents and humans. *J Clin Invest*. 2012;122(1):153-162.

Timper K, Denson JL, Steculorum SM, Heilinger C, Engström-Ruud L, Wunderlich CM, Rose-John S, Wunderlich FT, Brüning JC. IL-6 Improves Energy and Glucose

Homeostasis in Obesity via Enhanced Central IL-6 trans-Signaling. Cell Rep. 2017 Apr 11;19(2):267-280. doi: 10.1016/j.celrep.2017.03.043. PMID: 28402851.

Tran MD, Neary JT. Purinergic signaling induces thrombospondin-1 expression in astrocytes. Proc Natl Acad Sci U S A. 2006 Jun 13;103(24):9321-6. doi: 10.1073/pnas.0603146103. Epub 2006 Jun 5. PMID: 16754856; PMCID: PMC1482608.

Wang WY, Tan MS, Yu JT, Tan L. Role of pro-inflammatory cytokines released from microglia in Alzheimer's disease. *Ann Transl Med*. 2015;3(10):136. doi:10.3978/j.issn.2305-5839.2015.03.49

WEIR JB. New methods for calculating metabolic rate with special reference to protein metabolism. J Physiol. 1949 Aug;109(1-2):1-9. doi: 10.1113/jphysiol.1949.sp004363. PMID: 15394301; PMCID: PMC1392602.

Yo Sasaki, Keiko Ohsawa, Hiroko Kanazawa, Shinichi Kohsaka, Yoshinori Imai, Iba1 Is an Actin-Cross-Linking Protein in Macrophages/Microglia, Biochemical and Biophysical Research Communications, Volume 286, Issue 2, 2001, Pages 292-297, ISSN 0006-291X.

Young, J.K. (2002), Anatomical relationship between specialized astrocytes and leptin-sensitive neurones. Journal of Anatomy, 201: 85-90.

Zhao Y, Zhao Y, Zhang M, et al. Inhibition of TLR4 Signalling-Induced Inflammation Attenuates Secondary Injury after Diffuse Axonal Injury in Rats. *Mediators Inflamm*. 2016;2016:4706915. doi:10.1155/2016/4706915.

7. Annex

7.1 In vitro culture of astrocyte of DIO and DR males after 1 day, 3 days or 4 days FA treatment: measures of cytokine production

The results presented in this supplementary chapter (**Fig. A1-2**) refer to experiment 2 of the study and were obtained from the primary cultures of hypothalamic astrocytes harvested from 3-week-old male DIO and DR rats. While, DR astrocytes showed a nice dose-response, DIO astrocytes did not show an increase in cytokine concentration after the start of treatment. Therefore, this does not allow us to compare the two groups. These results are quite surprising compared to female astrocytes and we do not know if DIO male primary astrocytes secrete much less cytokines in general. Thus this experiment needs to be repeated to confirm this results.

Some possible reasons that would explain the results obtained from the culture of DIO male astrocytes are: 1) these cells were used after the 2nd passage while female astrocytes were used after the 1st passage, thus it may be that this extra passage made these primary astrocytes to lose their phenotype. However, this would not explain the difference between DR and DIO; 2) another possible explanation is that the cells didn't react to the treatment because they died. This is improbable, as we checked them daily and did not observe any decrease in cell count; 3) the last possible explanation is that DIO male astrocytes reacted by producing less cytokines in comparison to the other groups we tested. This hypothesis needs to be further investigated.

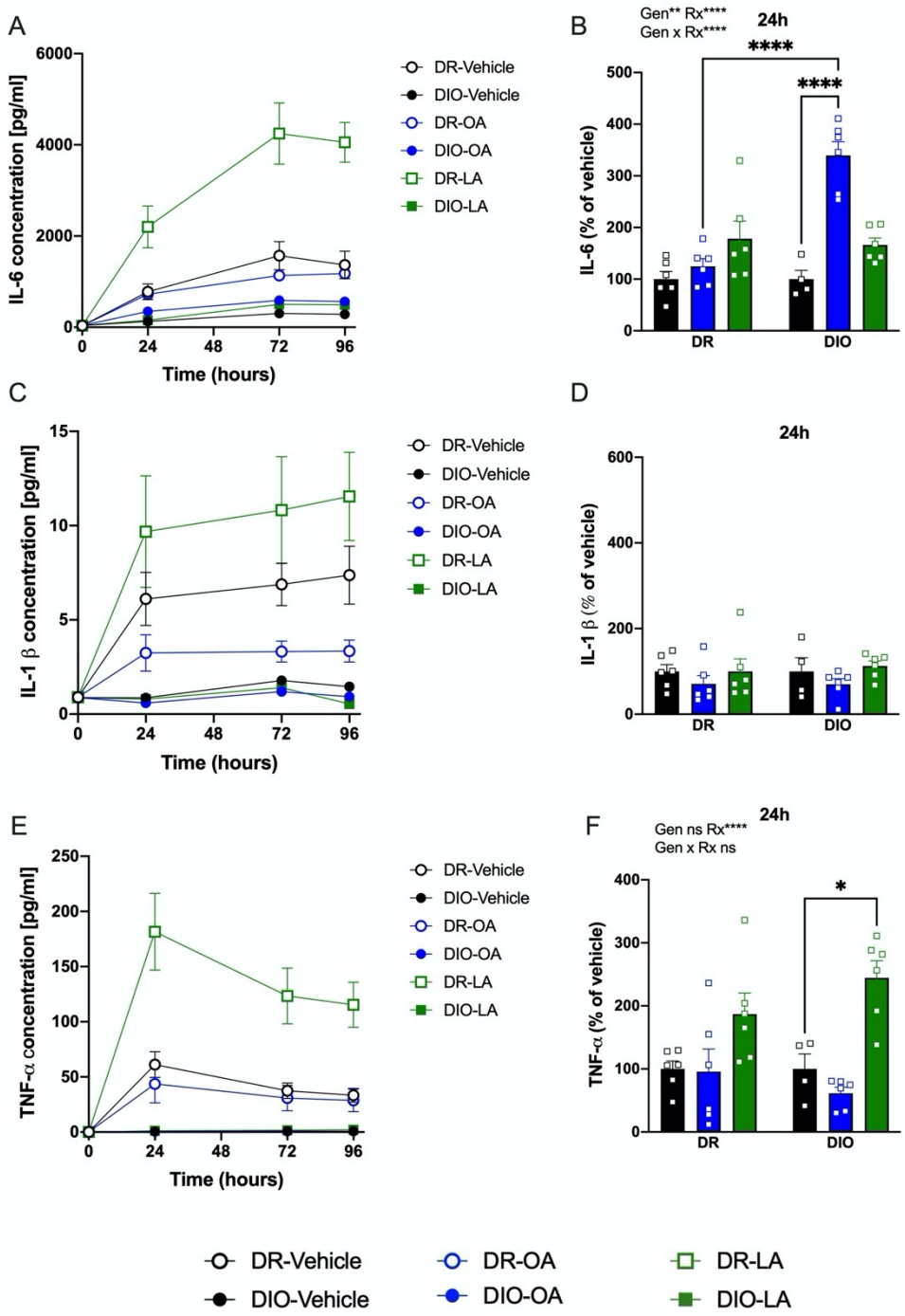

Figure A1: Effect of unsaturated fatty acid (FA) exposure on ventromedial hypothalamus (VMH) astrocyte cytokine production in chow fed DIO and DR rats. IL-6 (pg/ml) (A, B), IL-1β (pg/ml) (C, D) and TNF-α (pg/ml) (E, F) concentration in media harvested from the culture of male DIO and DR astrocytes that were treated for 96 hours with either 13 μM oleic or linoleic acid (or the same volume of media in the vehicle treated group) (A, C, E). B; D; F: concentration of cytokines 24h after the first treatment expressed as percent of vehicle.All data are expressed as mean ± SEM; n = 5-6/group. Statistics: ns > 0.05; *P ≤ 0.05; **P≤0.01; ***P≤0.001; ****P≤0.0001 by 2-way ANOVA. (a, b, c) Data points with different superscript at each time point differ from each other by P<0.05 after multiple comparison intergroup analysis.

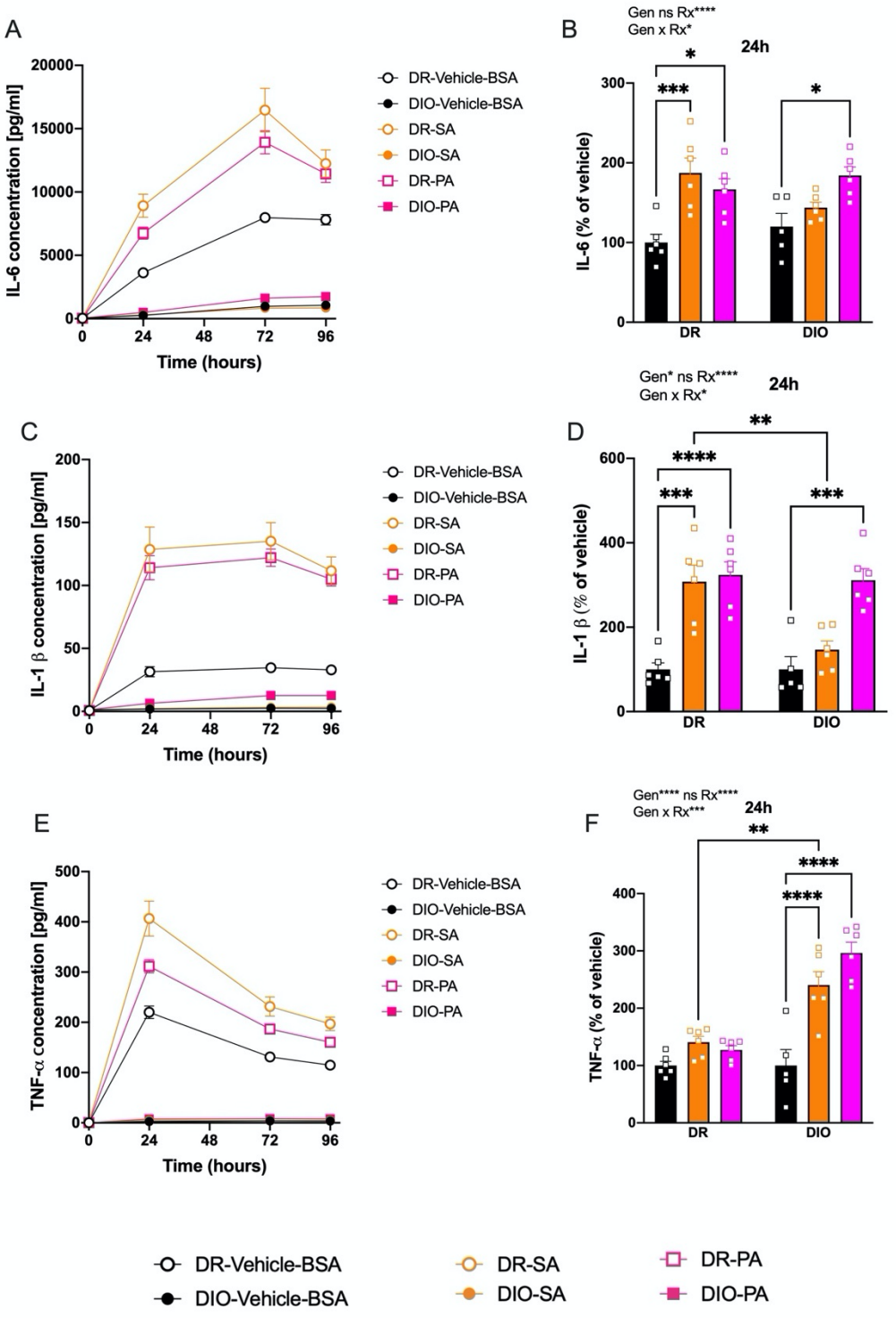

Figure A2: Effect of saturated fatty acid (FA) exposure on ventromedial hypothalamus (VMH) astrocyte cytokine production in chow fed DIO and DR rats. IL-6 (pg/ml) (A, B), IL-1β (pg/ml) (C, D) and TNF-α (pg/ml) (E, F) concentration in media harvested from the culture of male DIO and DR astrocytes that were treated for 96 hours with either 73 μM palmitic or stearic acid (or the same volume of media in the vehicle treated group) (A, C, E). B; D; F: concentration of cytokines 24h after the first treatment expressed as percent of vehicle. All data are expressed as mean ± SEM; n = 5-6/group. Statistics: ns > 0.05; *P ≤ 0.05; **P≤0.01; ***P≤0.001; ****P≤0.0001 by 2-way ANOVA. (a, b, c) Data points with different superscript at each time point differ from each other by P<0.05 after multiple comparison intergroup analysis.

8. Acknowledgements

I would like to thank the whole research group under Prof. Dr. Thomas Lutz for the great atmosphere and for their helpfulness. In particular, my supervisor Christelle Le Foll, PhD, for providing patient guidance and feedback throughout this project.

I want to thank Prof. Dr. Thomas A. Lutz for giving me the wonderful opportunity to do my Dissertation in his lab. It was a privilege for me to work with your team.

I also want to thank Dr. Christina Neuner Boyle, who always supported me.

Last but not least many thanks go to Sarah Benz for her help with the animals.

9. Curriculum Vitae

Vorname Name	Luca Papini
Geburtsdatum	06.12.1993
Geburtsort	Lugano
Nationalität	Schweiz
Heimatort bei Schweizer/-in	Diepoldsau-Schmitter SG
September/2008 – Juni 2012	**Liceo Cantonale di Lugano 1** 6900 Lugano, TI, Schweiz
26. Juni 2012	**Matura** Liceo Cantonale di Lugano 1, 6900 Lugano, TI, Schweiz
September/2013 – Dezember/2019	**Veterinärmedizin** Universität Bern, 3012 Bern, Schweiz
30. Dezember 2019	**Abschlussprüfung vet. med.** Universität Bern, 3012 Bern, Schweiz
Februar/2020 – Januar 2021	**Anfertigung der Dissertation** unter Leitung von Prof. Dr. med. vet. Thomas Lutz und Dr. Christelle Le Foll am Institut für Veterinärphysiologie der Vetsuisse-Fakultät Universität Zürich Direktor: Prof. Dr. med. vet. Max Gassmann
Februar/2021 – Heute	**Internship** ISME Pferdeklinik, 3012 Bern, Schweiz